March 1986 LS-52

6 GeV Synchrotron X-Ray Source Conceptual Design Report

Supplement A

Characteristics of the Insertion Devices for the 6 GeV Synchrotron Source

Argonne National Laboratory, Argonne, Illinois 60439
operated by The University of Chicago for the U. S. Department of Energy under Contract W-31-109-Eng-38

DISCLAIMER

SUPPLEMENT A

CHARACTERISTICS OF THE INSERTION DEVICES FOR THE 6 GeV SYNCHROTRON SOURCE

MARCH 1986

TABLE OF CONTENTS

LIST OF FIGURES

LIST OF FIGURES (Cont'd)

LIST OF TABLES

1 Introduction

Historically, synchrotron radiation (SR) has been obtained primarily from bending-magnet (BM) sources. These continuous sources of electromagnetic radiation have contributed in a major way to our understanding of the structure and dynamics of biological, chemical and material systems. During the past few years, newer sources of SR based on sophisticated periodic magnetic structures, called insertion devices (IDs), have been developed. The electromagnetic radiation from these IDs can be used as a very versatile probe in scientific and technological research which is far superior to that based on a BM source.

Two different types of IDs--undulators and wigglers--have been developed to satisfy the requirements of various investigations. These requirements include the need for radiation with specific polarization characteristics, a micrometer-sized source, extremely narrow emanation of the radiation (low divergence), tunability of the energy of the radiation, ultrahigh spectral brilliance covering an x-ray energy range from soft to hard, and a matching of the radiation characteristics with those of the x-ray optical elements for maximum utilization of the potential of such sources. All these can be provided by a proper match between the characteristics of the positron beam in the storage ring and the ID characteristics. Unlike the IDs presently retrofitted on existing storage rings, the IDs on the Argonne 6 GeV storage ring will be optimized in every aspect of their performance to form an integral part of the design and to meet the specific needs of the research programs that are planned and proposed for this storage ring. On the other hand, as experience is gained in the use of ID radiation, new applications will emerge. Hence, it is essential that the integral design of the storage ring and the insertion sections be flexible enough to accommodate

future needs. The design of the storage ring described in the previous sections incorporates this flexibility.

The primary purpose of the 6 GeV Light Source is to provide ID-based sources. However, it can also deliver BM radiation. It is anticipated that in view of excessive requests for beam time for hard x-rays on various synchrotrons in the U.S., the 6 GeV Light Source will be in demand for its BM radiation. Also, there are many situations where high-energy radiation is extremely useful, but the sample cannot take the excessive radiation power from an ID. The 6 GeV BM radiation is well suited to such situations.

2 Undulator, Wiggler, and Bending-Magnet Sources

As indicated earlier, 64 BMs are used in the storage ring to keep the positrons in a nearly circular orbit. We can extract SR from 32 of these BMs. There are 32 straight sections between the BMs in which one can introduce the IDs. These devices provide great flexibility in tailoring the characteristics of the emerging radiation to suit the needs of specific research programs. The positrons traveling along the length of such an ID experience transverse motion due to periodic magnetic fields that alternate in their polarity. The spectral distribution from this motion of the positrons can be continuous and wide, in which case the ID is called a "wiggler." On the other hand, the emitted radiation can have spectrally narrow and discrete peaks, in which case the ID is called an "undulator." The distinction between wigglers and undulators is determined quantitatively by the value of the so-called deflection parameter K. If the motion of the positron in a transverse ID is approximately sinusoidal, then K is given by

$$K = 0.934\ B_o\ \lambda_o, \quad (1)$$

where B_o is the peak magnetic field in tesla and λ_o is the spatial period of the magnetic structure in centimeters. When $K \geq 10$, the device is called a wiggler and each of the magnetic poles of the wiggler acts as an independent radiation source similar to a BM. The number of poles (or magnetic periods) in such a "multipole wiggler" determines the degree to which the photon intensity (or total flux) will be enhanced. One can also increase the energy of the photons from such a device by proper choice of B_o. The photon critical energy, E_c, for the 6 GeV ring is given by

$$E_c \text{ (keV)} = 23.95\ B_o. \tag{2}$$

There are situations when one merely wants to increase the photon energy without increasing the total radiated power from a wiggler. This is accomplished by designing a wiggler made up of a single magnetic period with a large magnetic field B_o. Such a wiggler is usually referred to as an "energy-shifter." On the other hand, there are situations where one would prefer to have a high-flux wiggler with a low value of E_c. This is of special interest in applications where higher photon harmonics are detrimental to the success of the investigation. This so-called "low-E_c" wiggler can be designed by incorporating multiple periods with low B_o.

For cases with $K \leq 1$, the radiation from various poles of an undulator shows constructive interference effects, which produce a spectrum consisting of one or several (harmonic) peaks. Because of the compression of radiated energy into these narrow peaks, one can realize very large photon fluxes in an energy range of choice from undulators. This should be contrasted with the radiation from wigglers or BMs, which deliver useful radiation as well as a large percentage of unwanted radiation from their

continuous spectral distributions. The unwanted radiation can form a large heat load on the first optical element and hence complicate its design. This situation is alleviated by the use of undulator radiation.

It must be pointed out that in spite of their attractive characteristics, undulators cannot cater to all experimental needs. It is hard to obtain first-harmonic radiation of more than 20 keV energy from an undulator on a 6 GeV synchrotron with the presently available magnet technology. Also, the energy tunability of radiation from undulators is somewhat less straightforward than that from wigglers and BMs.

Instead of a transverse motion of positrons in the ID, one can have helical motion. The characteristics of radiation emitted by such a helical ID are somewhat different from that emitted by a transverse device. The helical devices, however, perturb the storage ring beam in a major way. Hence we shall limit our discussion in this proposal primarily to transverse IDs.

The IDs are so designed that the total magnetic-field integral over their length is zero, and hence their presence does not alter the ideal closed orbit in the storage ring. In fact, the influence of IDs on the positron trajectory is an order of magnitude less severe than that from BMs. This provides an unprecedented flexibility to incorporate IDs with different radiation characteristics without a detailed reevaluation of the storage ring performance, whereas the character of the radiation from the BMs cannot be tailored as desired.

3 Source Size, Brilliance, Brightness, and Flux

Three quantities can be used to characterize the radiated photon beam from any of the above-mentioned sources on a storage ring. They are the "photon flux," "spectral brilliance," and "spectral brightness." The photon

flux is defined as follows:

$$\text{photon flux} = \text{number of photons/sec/0.1\%BW/mrad } \theta, \tag{3}$$

where BW is bandwidth and θ is the angular spread of the radiation in the orbital plane. Equation (3) represents the integrated number of photons over the entire vertical opening angle ψ. The spectral brilliance is the spectral intensity emitted in the unit phase-space volume of the radiation field, and is expressed in the following units:

$$\text{spectral brilliance} = \text{number of photons/sec/0.1\%BW/mrad}^2/\text{mm}^2. \tag{4}$$

The phase-space volume is obtained by convoluting the Gaussian distribution describing the positron beam in a storage ring and the radiation field described in terms of Gaussian optics. If Σ_i and Σ_i' (i=x,y) are beam size and divergence, the average value of spectral brilliance over the length of the device is obtained by dividing the photon flux by $4\pi^2\Sigma_x\Sigma_y\Sigma_x'\Sigma_y'$.

In a straight section containing an undulator, the effective size and the divergence of the source, Σ_i and Σ_i' (i=x,y), are given by

$$\Sigma_i = (\sigma_R^2 + \sigma_i^2)^{1/2}; \quad \Sigma_i' = (\sigma_R'^2 + \sigma_i'^2)^{1/2}. \tag{5}$$

Here σ_R and σ_R' are the source size of the radiation field and the opening angle of the radiation, respectively. The quantities σ_R and σ_R' are functions of the radiation wavelength λ and undulator length L, and they include depth-of-field and/or diffraction effects; they are given by

$$\sigma_R = \frac{1}{4\pi}\sqrt{\lambda L}\ ; \quad \sigma_R' = \frac{\lambda}{L}\ . \tag{6}$$

In Eq. (5), σ_i and σ_i' (i=x,y) are the positron beam size and divergence. These quantities are functions of the emittance of the lattice and the value of the amplitude function β (betatron functions). As pointed out earlier, the values of β are determined by the focusing properties of the storage ring lattice and will be different in various sections of the ring. The emittances in the orbital (horizontal) plane (ε_x) and vertical plane (ε_y) are given by

$$\varepsilon_x = \frac{\varepsilon_o}{1 + k^2}\ ; \quad \varepsilon_y = \frac{\varepsilon_o k^2}{1 + k^2} \tag{7}$$

where $\varepsilon_o = 8.0\text{x}10^{-9}$ m•rad is the natural emittance of the proposed 6 GeV lattice and k^2 is the xy coupling parameter. With positron beam coupling in the x-y plane defined by $k^2 = 0.1$ (for the lattice), we obtain

$$\varepsilon_x = 7.3\text{x}10^{-9}\ \text{m•rad}; \quad \varepsilon_y = 7.3\text{x}10^{-10}\ \text{m•rad}. \tag{8}$$

In terms of the betatron functions β_x and β_y, the rms Gaussian width and divergence of the positron beam are given by

$$\sigma_i = \sqrt{\varepsilon_i \beta_i}\ ; \ \sigma_i' = \sqrt{\varepsilon_i / \beta_i} \quad (i=x,y). \tag{9}$$

It is clear that the effective phase-space volume is dependent on the betatron functions for a device of fixed length in a storage ring, although this dependence is rather insensitive at short wavelengths of photons. (Mathematically, there exists a set of optimum betatron functions for which the phase-space volume is minimum and the brilliance is maximum.

This occurs for $\beta_x = \beta_y = L/2.$) Hence, for all practical purposes the undulator brilliance is independent of betatron functions. On the other hand, in situations where one desires low photon-beam divergence, one should maximize β_x and/or β_y as much as the lattice operation will permit. Through an evaluation of the needs of various experiments that will use the undulator and wiggler sources, it is found that the undulators should be low-divergence devices whereas the wigglers could be optimized for high brilliance. On the basis of these general guidelines, the values of β_x and β_y in various parts of the lattice have been chosen. In Table 1, we present the values of betatron functions, positron beam size, and beam divergence in various parts of the proposed lattice in the absence of any insertions. It is important to note that in the design and operation of the storage ring, there exists considerable flexibility with regard to the choice of β_x and β_y values, since the optimum values cover a broad range.

There are some important observations that are specific to the 6 GeV lattice: (1) The effective size of the source (Eq. 5) is fairly independent of photon energies larger than about 1 keV. (2) In the same energy range, the apparent source size and divergence due to radiation are smaller than the same quantities for the positron beam. For 1 Å (or 12 keV) radiation from a 5 m long undulator, $\sigma_R = 1.8$ μm and $\sigma'_R = 4.5$ μrad. Thus, $\sigma_R < \sigma_i$ and $\sigma'_R < \sigma'_i$ $(i=x,y)$. Hence, σ_R and σ'_R make no major contribution to the total source size. The positron beam size and beam divergence mainly govern the spectral characteristics of the radiation from the various sources on the 6 GeV storage ring.

Finally, there are experimental situations where the physical size of the source is of no importance and beam need not be focused onto the sample. In such situations, the useful quantity to characterize the radiation

beam is "spectral brightness." We define this as the brilliance integrated over the source size and express it in photons/sec/0.1%BW/mrad^2. High brightness is achieved when the beam has small divergence.

Table 1

Betatron Functions, Positron Beam Size,and Positron Beam Divergence in Different Parts of the Proposed 6 GeV Lattice

	Bending Magnet	Undulator	Wiggler
β_x (m)	0.92	22.5	1.37
β_y (m)	24.4	13.15	1.24
σ_x (μm)	82	405	100
σ_y (μm)	133	98	30
σ'_x (μrad)	89	18	73
σ'_y (μrad)	5	7	24

4 General Characteristics of Radiation Sources on the 6 GeV Ring

In this section we will summarize the nature of radiation from bending magnet, undulator, and wiggler sources on a 6 GeV storage ring and compare them with those from the sources on presently operating storage rings.

4.1 Bending Magnet Sources

In the present design of the storage ring with 64 BMs, the radiation from each bend covers 98.17 mrad and the trajectory of the positrons through each bend has a radius of 25 m. The vertical opening angle 2ψ of this radiation sheet is approximately $2/\gamma$, where γ is the relativistic enhancement of the positron rest energy. For the 6 GeV lattice, $\gamma = 11742$. Hence, the value of $2/\gamma$ is about 170 μrad.

The radiation from a BM source has a uniform distribution in the horizontal (xz) plane. The complete spectral brilliance, BR, of the BM source as a function of the vertical opening angle and the photon energy E (in keV) is given by

$$BR(E,\psi) = 1.32 \times 10^{10} \; I \; E_R^2 \; E^2 \; F(\gamma\psi)/E_c^2, \tag{10}$$

where BR is in the usual units for spectral brilliance (see Eq. (4)), I is the total positron current in mA, E_R is the storage ring energy in GeV, and E_c is the critical energy (in keV) given by Eq. (2); E_c has a value of 19.16 keV for the BMs on this lattice ($B_o = 0.8$ T). The function $F(\gamma\psi)$ is given by

$$F(\gamma\psi) = (\gamma\psi)^2 \; [1 + (\gamma\psi)^2] \; K_{1/3}^2(\xi) + [1 + (\gamma\psi)^2]^2 \; K_{2/3}^2(\xi), \tag{11}$$

where

$$\xi = (E/2E_c) \; [1 + (\gamma\psi)^2]^{3/2}. \tag{12}$$

The central spectral brilliance is obtained by evaluating Eq. (10) with $\psi = 0$. In Eq. (11), $K_{1/3}$ and $K_{2/3}$ are Bessel functions of fractional order.

If one collects the radiation over the entire vertical angle ψ, the integrated spectrum per unit azimuthal angle θ gives the flux:

$$f(E) = 2.456 \times 10^{10} E_R I E G(y)/E_c \quad (13)$$

where f is in ph/sec/0.1%BW/mrad θ, E_R is in GeV, I is in mA, E and E_c are in keV, and the function G(y) is defined by

$$G(y) = \int_y^\infty K_{5/2}(x)dx, \quad y = E/E_c. \quad (14)$$

In Fig. 1, the relationship given in Eq. (10) is used to plot the brightness of the BM source as a function of vertical opening angle ψ for various values of the photon energy E. It should be noted that at low energies (<2 keV), the radiation spreads well above $2/\gamma$ (= 1.7×10^{-4} rad). The radiation obtained with $E = E_c$ carries maximum brightness. One notices from the figure that the soft x-ray radiation (< 2 keV) has considerable brightness for $\psi > 2/\gamma$. In order to profitably use these soft x-ray photons, schemes have been developed to shield the high-energy radiation by a cooled in-plane mask and to collect the soft x-ray radiation by using appropriate optics based on metallic superlattice structures.

Table 2 compares the parameters of BM sources on the 6 GeV storage ring with those of several operating hard x-ray storage rings. The list includes design parameters (which may not correspond to operating parameters) for the National Synchrotron Light Source (NSLS) located at the Brookhaven National Laboratory in New York; the Stanford Synchrotron Radiation Laboratory (SSRL), which uses the SPEAR storage ring at Stanford University in California, and the Cornell High Energy Synchrotron Source (CHESS), which uses the CESR storage ring located at Cornell University in New York.

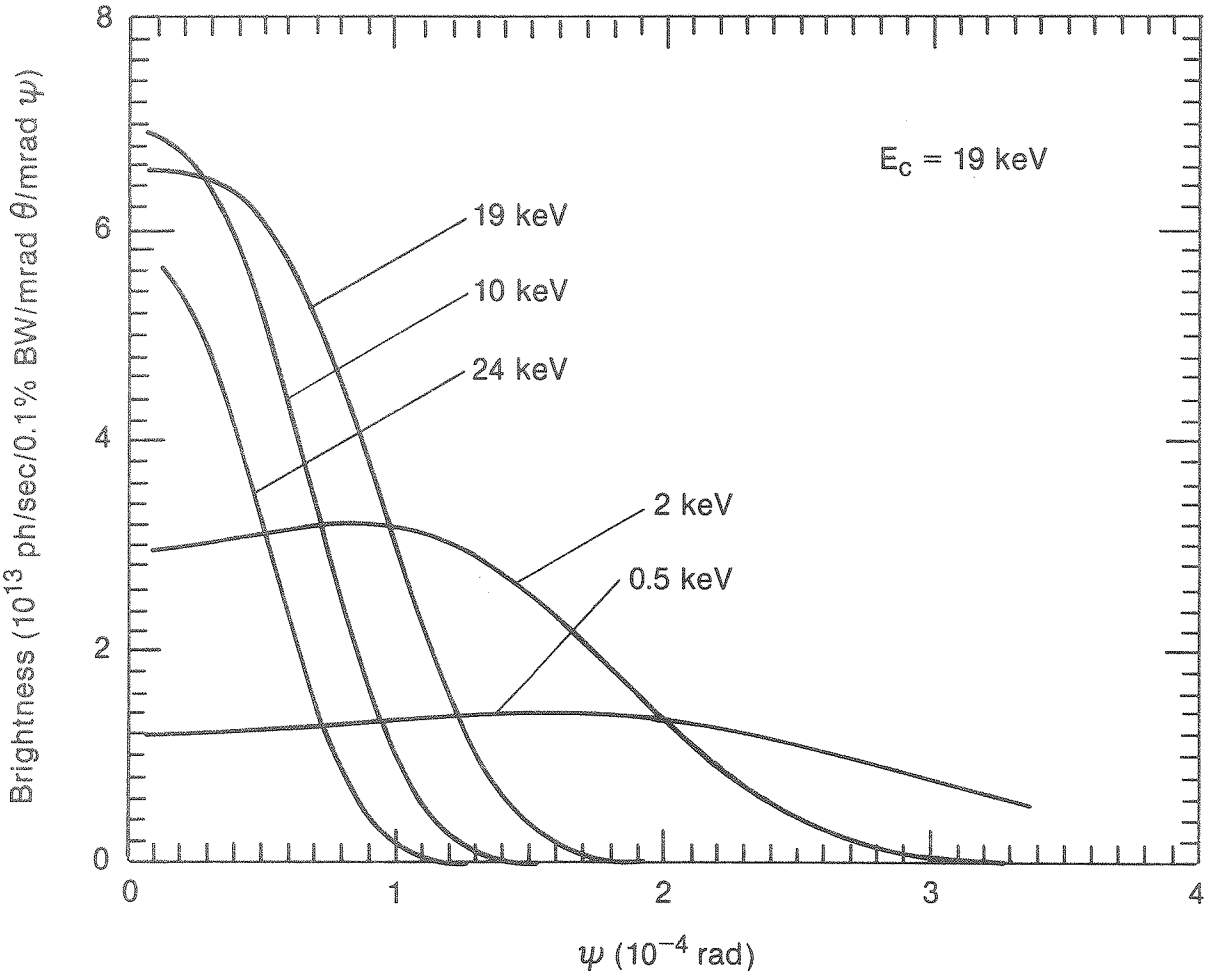

Fig. 1 Brightness of BM radiation from a 6 GeV storage ring (100 mA) as a function of vertical opening angle ψ for various photon energies

Table 2

Design Parameters of Various BM Sources

	6-GeV	NSLS	SSRL	CHESS
E (GeV)	6.0	2.5	3.0	5.5
I (mA)	100	500	100	40[a]
ρ (m)	30.0	6.8	12.7	32.0
B (T)	0.80	1.22	0.79	0.57
E_c (keV)	19.2	5.1	4.7	11.5
flux at E_c [b]	0.96	2.4	0.48	0.35
σ_x (mm)	0.082	0.3	2.0	1.44
σ_y (mm)	0.133	0.1	0.28	1.0

[a] CHESS is being upgraded to a current of 80 mA.

[b] In units of 10^{13} ph/sec/0.1%BW/mrad θ.

In Figs. 2 and 3, we have used the parameters of Table 2 to compare the flux and central spectral brilliance, respectively, from BMs on the 6 GeV source and three other sources. It is clear that among these sources the 6 GeV source has the highest flux for radiation with energies above about 7 keV; moreover, the 6 GeV source has the highest central brilliance over the rest over the whole spectral range.

4.2 Undulator Sources

Undulators can provide a very bright, quasi-monochromatic photon beam. The most prominent feature of the Argonne 6 GeV Light Source design is

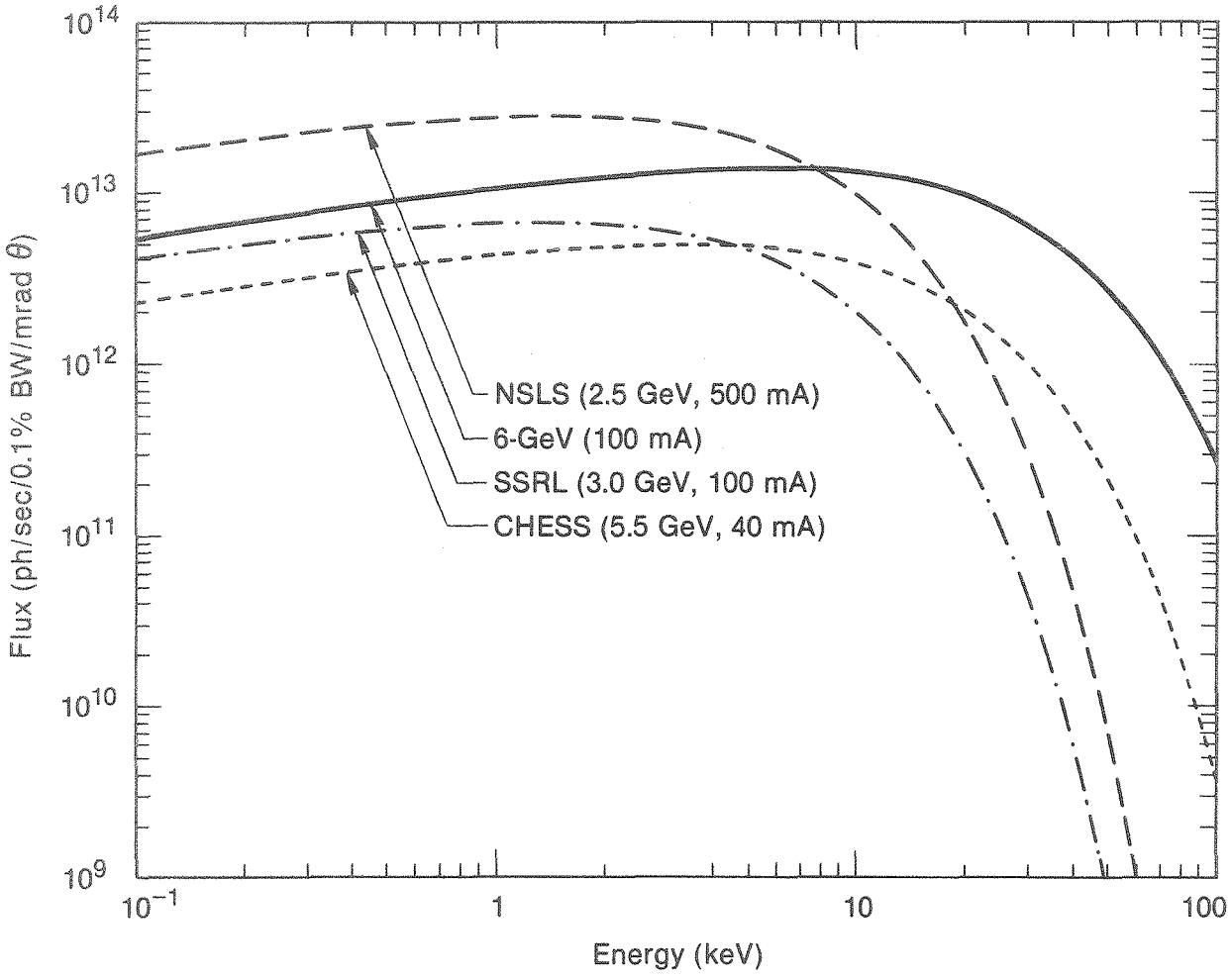

Fig. 2 Flux from BMs on various synchrotron sources

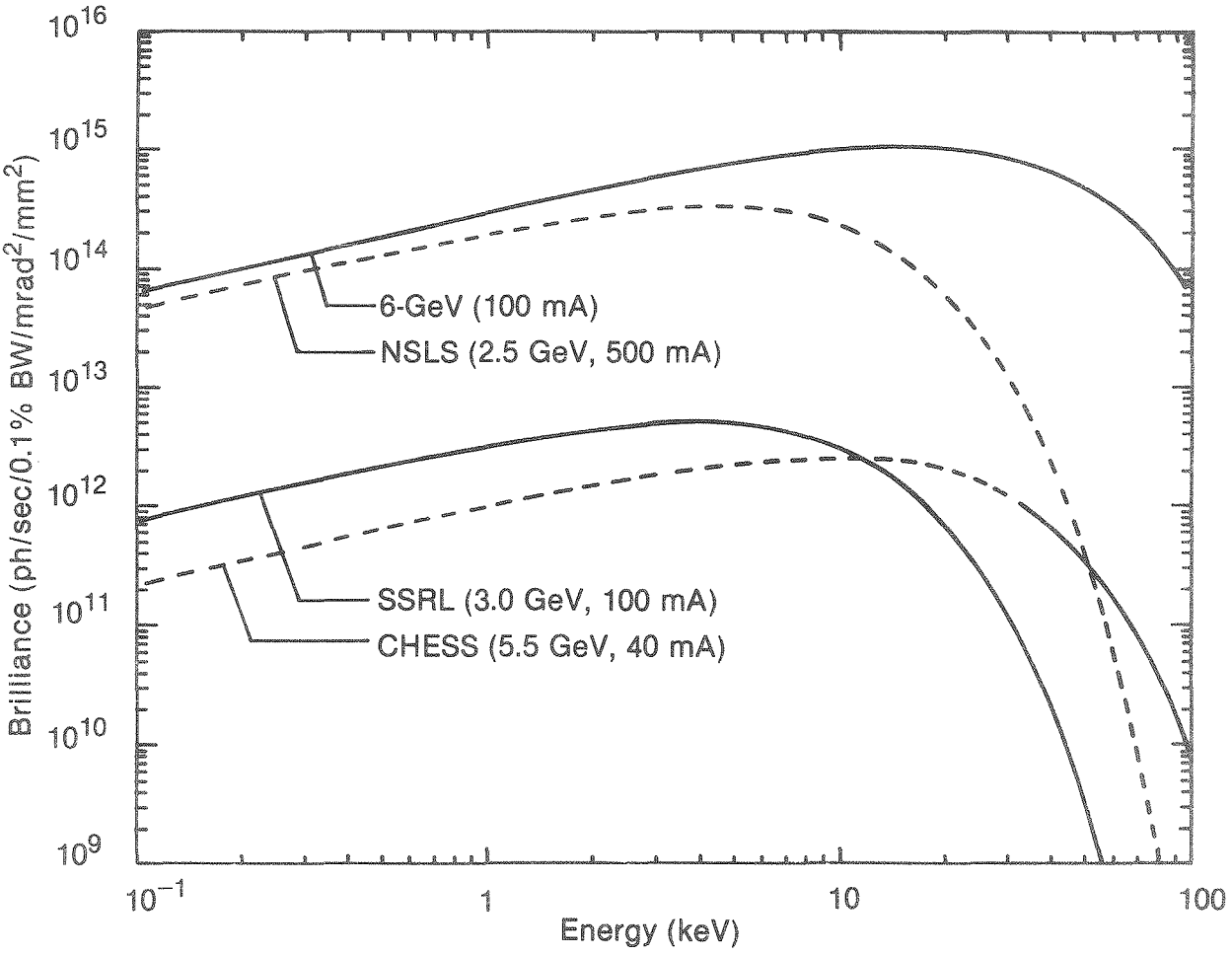

Fig. 3 Brilliance of bending magnet radiation of 6 GeV Light Source compared with those from other synchrotron sources in the U.S.

the large number of straight sections for such undulators. Out of 32 straight sections, as many as 28 will be available for the IDs after 4 are used for the accelerator components. The emittance of the present lattice has been carefully minimized and the betatron functions have been increased in the undulator straight sections to provide a low-divergence photon beam of high brilliance. The photon energy of the nth harmonic at an observation angle θ (in radians) relative to the undulator axis is given by

$$E_n = \frac{949\ E_R^2 n}{\lambda_o(1 + K^2/2 + 2\theta^2)}\ , \tag{15}$$

where E_n is in eV, E_R is in GeV, and λ_o is in cm. On axis ($\theta = 0$),

$$E_n = \frac{949\ E_R^2 n}{\lambda_o(1 + K^2/2)}\ , \quad n = 1,3,5,\ldots\ldots, \tag{16}$$

and only the odd harmonics are present. However, one will observe the even harmonics of radiation even along the axis if either (a) the pinhole along the axis has a finite size or (b) the positron beam has a finite size and divergence.

The minimum period of an undulator magnetic structure can be about 1.6 cm with modern-day magnet technology (see later discussions). Thus, from Eq. (16), it is easy to recognize that the highest first-harmonic energy that one can realize from an undulator on the 6 GeV storage ring will be about 20 keV. The analogous value for the NSLS is about 3 keV. Thus, the 6 GeV source is unique in providing undulator radiation in the hard x-ray range.

The average spectral brilliance or the flux from an undulator can be calculated to various degrees of precision. These procedures are described in more detail in Ref. 1. Our experience with a large number of such procedures

to compute the spectral brilliance has led us to accept the most realistic and accurate methodology, which is based on numerical integration procedures. In this method, the Lienard-Wiechert potential is integrated over a positron trajectory of finite dimensions. These procedures demand considerable computational time, depending on various parameters such as the number of periods in the device, the storage ring energy, the source dimensions, and the integration accuracy.

Figure 4 shows energy spectra for a typical 6 GeV undulator with a first-harmonic peak energy of ~11 keV. These calculations were done by the above-mentioned procedure, with the size and the divergence of the positron beam included, for undulators made of hybrid $SmCO_5$ (REC) magnets (see Section 6) and with the undulator parameters given in Table 3.

From Table 3 and Fig. 4, the following observations are made:

1. On-axis brilliance increases with increasing value of K, as expected from simple undulator theory.
2. Small values of K suppress the higher harmonics.
3. There is a fairly large contribution to the second-harmonic brilliance even when the radiation is collected along the undulator axis, because of the finite size of the positron beam.
4. The energy of the radiation peaks exhibits broadening and, as will be discussed below, this broadening is influenced by the non-zero-emittance beam of 6 GeV positrons.
5. The undulator can be tuned so that the first-harmonic energy can be varied between approximately 11 keV and 14 keV by varying the undulator gap between 1.2 cm and 2.0 cm, respectively. There is concurrent variation in the second- and third-harmonic energies and

this fact can be exploited in many experiments needing third-harmonic energy tunability.

6. The second- and third-harmonic radiation in most cases has higher brilliance than the BM brilliance.

The above discussion of a typical undulator provides a general understanding of the radiation characteristics from such sources. Later in this proposal, more details with respect to different devices will be provided.

Table 3

Parameters of the 6 GeV Undulator for Which the Undulator Energy Spectra of Fig. 4 Were Calculated

	Case A	Case B
Magnetic Gap, G (cm)	1.2	2.0
Undulator Period, λ_o(cm)	2.4	2.4
Peak Field On Axis, B_o (T)	0.34	0.11
Peak K On Axis	0.76	0.25
Number of Periods, N	208	208
Undulator Length, L (m)	5.0	5.0
1st-Harmonic Energy (keV)	10.987	13.813
1st-Harmonic Peak Brilliance[a] (10^{16})	265.0	40.20
2nd-Harmonic Peak Brilliance[a] (10^{16})	17.3	0.45
3rd-Harmonic Peak Brilliance[a] (10^{16})	24.6	0.07

[a]On-axis brilliance in ph/sec/0.1%BW/mrad^2/mm^2.

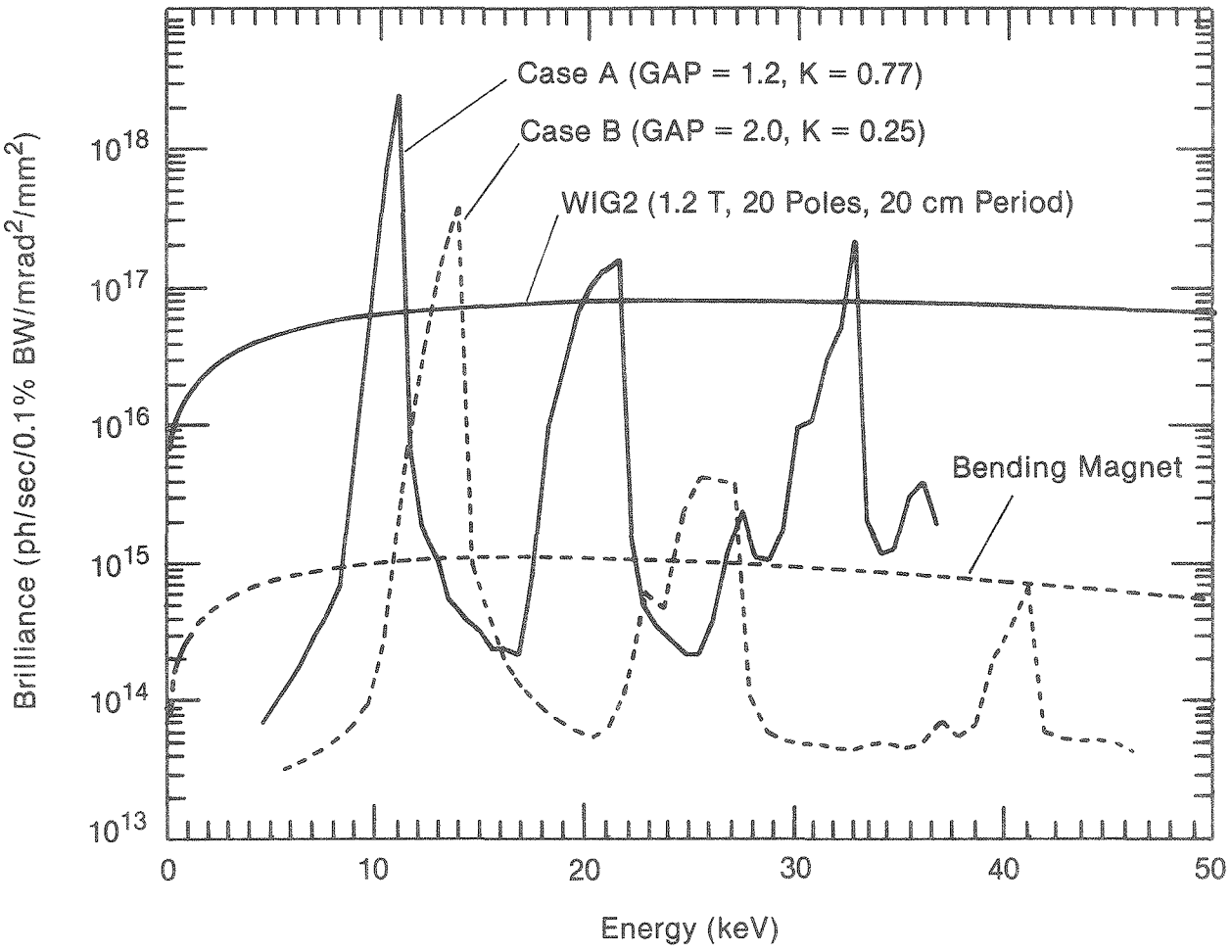

Fig. 4 Brilliance from an undulator (assuming two different magnetic gaps), compared with that from a wiggler and a BM source on a 6 GeV (100 mA) synchrotron

4.3 Wiggler Sources

In Section 2, we have defined various types of wiggler devices, namely, a multipole wiggler, an energy-shifter, and a low-E_c wiggler. Prerequisite for all these devices is a K value larger than about 10, which will result in a continuous and wide energy spectrum from them. This is achieved by having either large B_o and/or large λ_o. In principle, a multipole wiggler can supply the same number of photons per second in the same bandwidth as an undulator with an identical number of periods in the first harmonic. However, the opening angle of radiation and the effective source size for a wiggler are considerably larger than those of an undulator. Thus the spectral brilliance (or brightness) of a wiggler is lower than that of an undulator.

The flux of radiation from a multipole wiggler with N periods can be obtained by simply multiplying the expression for the flux from a BM, Eq. (13), by 2N. The central brilliance can also be calculated in a fashion similar to the BM case, if one is careful to use the proper source size. In Fig. 4, the central brilliance is plotted as a function of photon energy for a wiggler ("WIG2") defined by the following parameters: B_o = 1.2 T, λ_o = 20 cm, N = 10, and K = 22. The brilliance is also compared with that of the undulator discussed above, and with BM radiation. This wiggler source, with a critical energy of 28.7 keV, will be adequate for a large number of experiments requiring photon energies up to about 100 keV. As will be discussed later in detail, this wiggler can easily make use of permanent-magnet technology. It is hence important to recognize that for most conceivable applications of the 6 GeV source, there will be no need to use wigglers based on complex superconducting-magnet technology, of the type presently being designed and built for the NSLS.

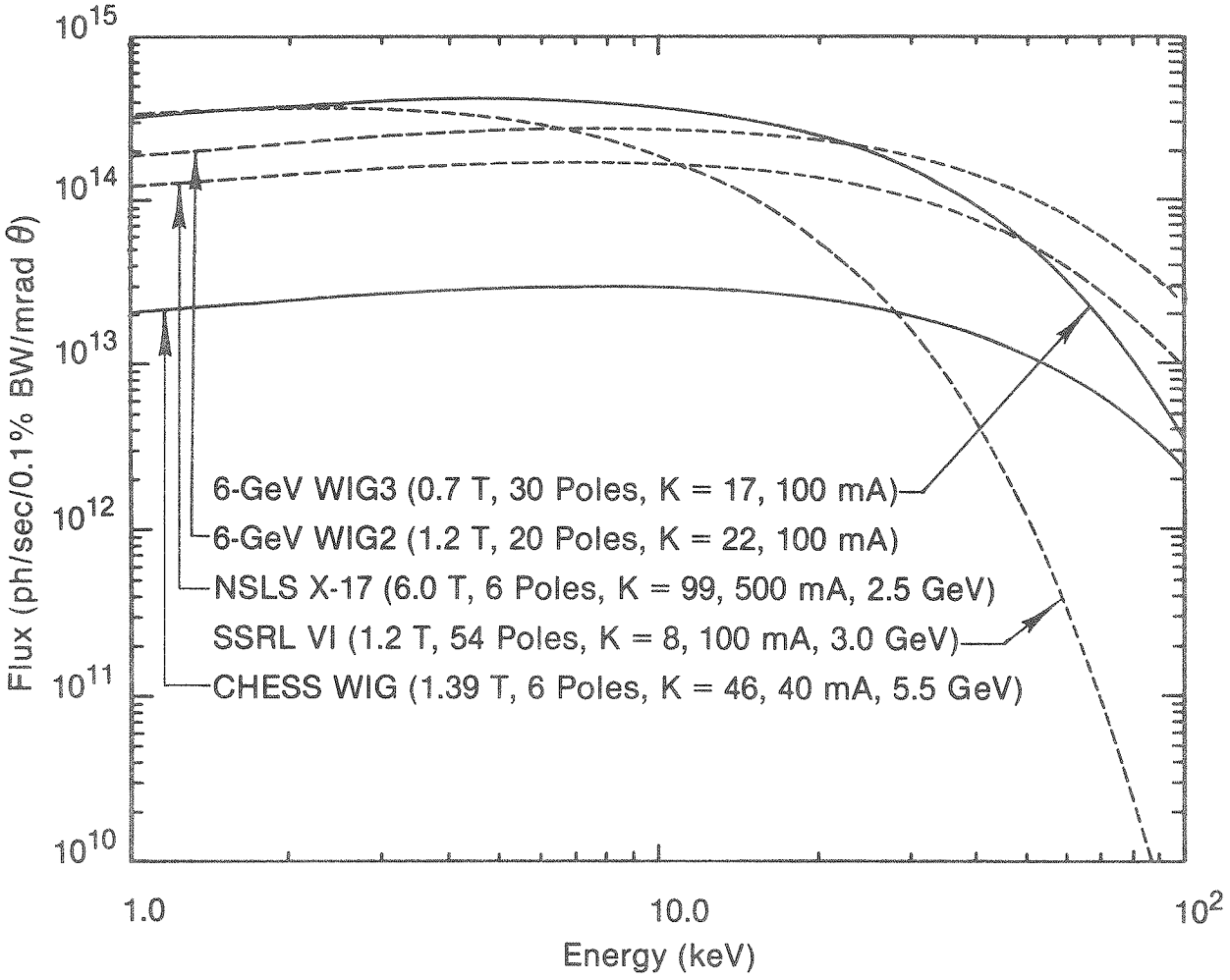

Fig. 5 Flux from wigglers on a 6 GeV (100 mA) storage ring, compared with those from wigglers on other synchrotron sources

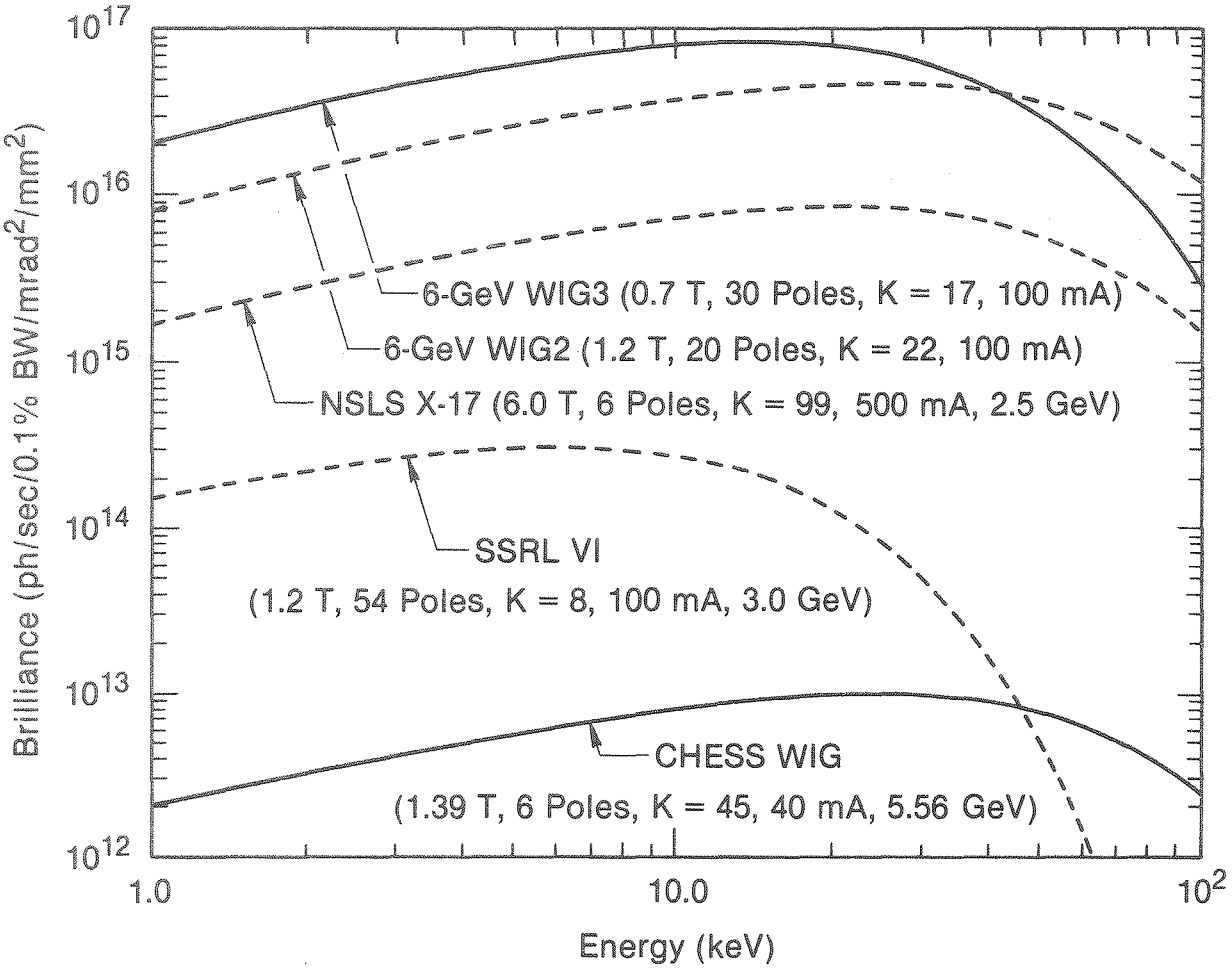

Fig. 6 Brilliance from wigglers on a 6 GeV (100 mA) storage ring, compared with those from wigglers on other synchrotron sources

It is useful to compare the performance of 6 GeV wigglers with those operating or planned on other storage rings. In Figs. 5 and 6 we present the dependence of flux and brilliance, respectively, for various wigglers as a function of photon energy. In arriving at these figures, the parameters given in Table 4 have been used.

Table 4

Parameters of Various Tranverse Wiggler Sources

	6 GeV WIG2	6 GeV WIG3	CHESS	SSRL VI	NSLS X-17
E_R(GeV)	6.0	6.0	5.5	3.0	2.5
I (mA)	100	100	40	100	500
ρ(m)	16.7	28.6	13.2	8.4	1.4
B_o(T)	1.2	0.7	1.39	1.2	6.0
σ_x(mm)	0.1	0.1	1.9	2.5	0.3
σ_y(mm)	0.03	0.03	1.2	0.15	0.02
E_c(keV)	28.7	16.8	27.9	7.16	24.9
Number of Poles	20	30	6	54	6
Period (cm)	20	10	35	7.25	17.8
K	22	7	45	8	99
L (m)	2.0	1.5	1.05	1.96	0.53
Total Power (kW)	6.5	1.7	1.6	1.6	37.9
Peak Power ($kW/mrad^2$)	16.7	14.6	1.6	2.8	3.8

5 Energy Spread in Undulator Peaks

For an undulator with N periods, the natural emitted bandwidth of the emitted radiation for an ideally parallel positron beam is given by

$$\Delta_1 = \frac{\Delta E_n}{E_n} = \frac{1}{nN} , \tag{17}$$

where n is the radiation harmonic. Thus, for a typical undulator with 200 periods, this bandwidth is 0.5% for the first harmonic. In the case of a 6 GeV ring with non-zero emittance, there are other sources of energy spread.

The contribution to the intrinsic bandwidth from the angular spread of the positron beam is

$$\Delta_2^i = (\sigma_i' \gamma)^2/(1 + K^2/2) , \quad i=x,y. \tag{18}$$

For an undulator straight section in the present lattice, we have (from Table 1) $\sigma_x' = 18$ μrad and $\sigma_y' = 7$ μrad. For a typical value of K = 0.3, the energy spreads along the x and y directions are 4.3% and 0.6%, respectively. Since the broadening effects along the two directions are not equal, the energy spread will be a convolution of these effects. The width at half maximum will be closer to the bandwidth in the y direction, and the distribution will have wings with spread closer to the bandwidth along the x direction.

The size of the positron beam also contributes to the energy spread. This can be estimated for a typical beamline length of D meters from the expression

$$\Delta_3^i = (\sigma_i/D)^2 \gamma^2, \quad i=x,y. \tag{19}$$

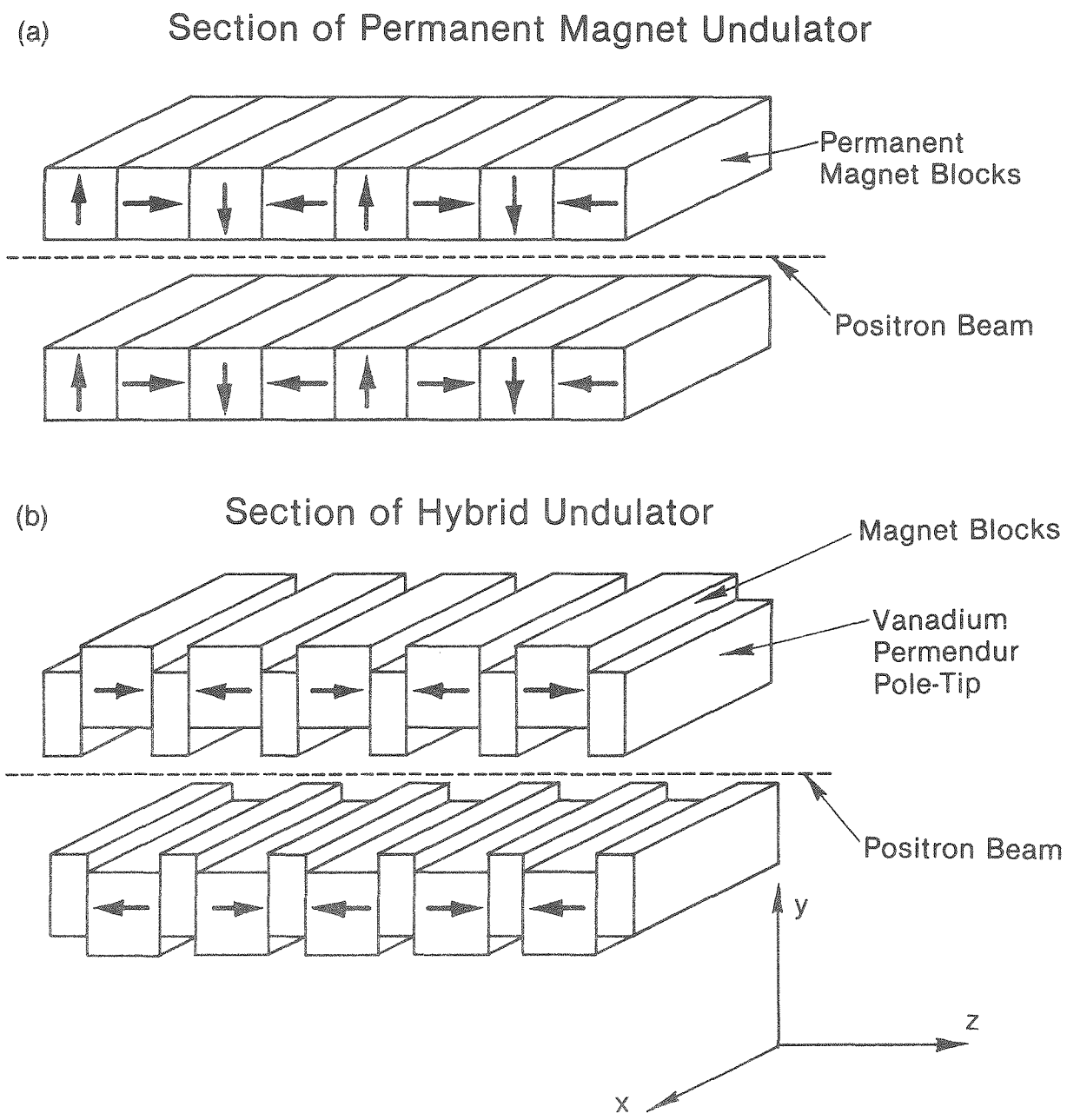

Fig. 7 Magnet configuration in (a) a permanent-magnet (CESM) undulator and (b) a hybrid undulator. The end-correction magnet configurations are not shown.

For our lattice with σ_x = 405 μm and σ_y = 98 μm, the bandwidths along the x and y directions will be 0.9% and 0.05%, respectively. This spread is small compared to that produced by the beam divergence.

All the above sources of intrinsic broadening of the energy peak add to produce a halfwidth of about 2%.

An additional extrinsic source of peak broadening is due to the acceptance angle, θ_o. The acceptance angle in an ideal situation can be set equal to σ_x', and this produces a bandwidth of $\gamma^2\theta_o^2$. For the proposed lattice, σ_x' = 18 μrad, which gives a broadening of 4.5%. This is the dominant contribution to the broadening of the peaks in Fig. 4.

6 Insertion Device Magnets and Gap

It has been pointed out that the IDs on the 6 GeV storage ring will not normally require superconducting magnets. The permanent-magnet technology for IDs is advancing very rapidly and many new undulator magnet design concepts are currently being developed. We foresee the following three types of magnet designs being considered for room-temperature transverse IDs:

Type 1: Permanent-magnet (CSEM) devices based on $SmCo_5$ (REC) or Nd-Fe-B material. A sketch of the geometry of such a device is shown in Fig. 7a.

Type 2: Hybrid magnet devices based on REC or Nd-Fe-B with the field-defining poles made of iron or vanadium permendur. The geometry of this configuration is shown in Fig. 7b.

Type 3: Electromagnetic devices assisted by active permanent-magnet materials.

The conceptual development of all these devices has taken place at the Lawrence Berkeley Laboratory, and we have benefited greatly from our contacts with the scientists and engineers involved. If a device were to be built today, the hybrid magnet device (type 2) would be the one of choice. These have considerable advantage over the permanent-magnet devices (type 1) because of their intrinsic ability to minimize construction errors in the in-plane magnetic field profile. The REC magnets have been used in some of the completed devices, but the Nd-Fe-B magnets will have a slight edge over REC magnets because of their higher remnant field. As a result, one can obtain the same peak field with a larger undulator gap if the magnets are Nd-Fe-B rather than REC. This is an important design consideration and will be discussed in detail below. A type 3 device based on combined electromagnets and permanent magnets has not yet been built. These devices will provide considerable flexibility and superior performance to meet the second-phase demands of the 6 GeV Light Source facility. Since more R&D is needed with respect to type 3 devices, for the purpose of this document we will limit our discussion mainly to transverse hybrid devices.

For the hybrid magnets based on permanent-magnet blocks and vanadium permendur pole-tips, the dependence of the peak magnetic field B_o on the magnet gap G (in cm) and undulator period λ_o (in cm) is given by the semi-empirical relationship

$$B_o(T) = 0.95a \exp\left[-G/\lambda_o(b - cG/\lambda_o)\right] \qquad (20)$$

In Eq. (20) the factor 0.95 represents the "filling factor" to account for losses in the field due to poor packaging of the high-permeability material in the undulator assembly. The equation is generally true for

$0.07 \leq G/\lambda_o \leq 0.7$. The values of the constants a, b, and c are given in Table 5 for REC and Nd-Fe-B hybrid magnets.

Table 5

Constants Used in Eq. (20), and Values of Remnant Field, for Hybrid Magnets Based on REC or Nd-Fe-B

	$SmCo_5$ (REC)	Nd-Fe-B
a	3.33	3.44
b	5.47	5.08
c	1.8	1.54
Remnant Field, B_r (T)	0.9	1.1

The important aspect of Eq. (20) is the inverse exponential dependence of B_o on the gap-period ratio, G/λ_o. Hence, as indicated earlier, the gap becomes an important factor determining B_o and, in turn, the value of K, which determines the character of the radiation emitted by an ID. In Section 4.2, we showed that in order to obtain 20 keV first-harmonic radiation from an undulator, λ_o has to be ~1.6 cm. For such short-period devices, to maintain G/λ_o less than 0.7, it is necessary to work with small gaps (0.9 cm). Reducing gaps to such small values is central to the detailed design of an ID.

In Fig. 8, Eq. (20) is used to plot the dependence of the peak magnetic field, B_o, on the gap-period ratio, G/λ_o, for REC and Nd-Fe-B hybrid magnets. Clearly, the Nd-Fe-B hybrid geometry provides a higher field than the REC hybrid geometry.

Next we will make a few observations on the mechanical properties of magnet materials. $SmCo_5$ (REC) is a mechanically brittle material, and preparing magnet blocks of a uniform size and geometry and with a highly homogeneous field distribution is difficult. This is of major concern in designing permanent-magnet (type 1) configurations. In the hybrid configuration, the mechanical tolerances are more critical for the pole-tips than for the magnet blocks. The pole material, namely, iron or vanadium permendur, has much better mechanical properties than REC or Nd-Fe-B, and hence the hybrid design is less affected by variations in the magnetization of REC or Nd-Fe-B blocks. In choosing between Nd-Fe-B and REC, two points of comparison are important in addition to the field comparison of Fig. 8: (1) Nd-Fe-B can be mechanically worked more easily than REC, and (2) the cost of Nd-Fe-B is considerably lower than that of the high-grade REC that is needed for a successful undulator design.

The above discussion leads us to conclude that the hybrid geometry, based on Nd-Fe-B magnets, should be the choice for 6 GeV applications. However, at present we have the following reservations:

1. The Curie temperature of Nd-Fe-B is much lower than that of REC and is only 150°C above room temperature. Hence, a large variation in the ambient temperature can alter the magnetization and thus the undulator characteristics.

2. For the same reason, a gradient in the temperature along the length of the undulator could also grossly affect the undulator radiation. Such

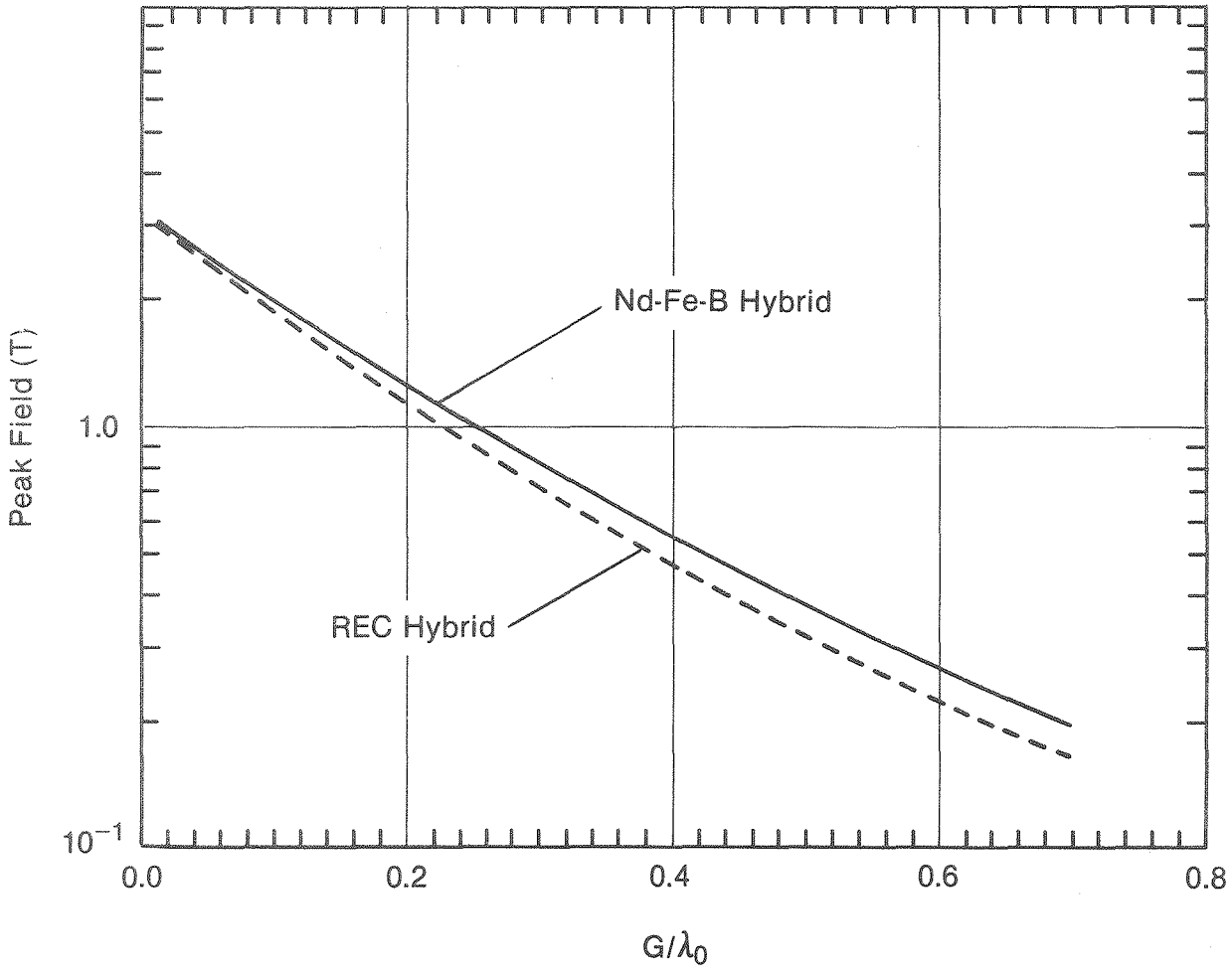

Fig. 8 Variation of peak field in a hybrid configuration with REC and Nd-Fe-B magnets as a function of G/λ_o

temperature gradients can come about if the radiation hits the walls of the ID vacuum chamber on which the magnet poles are resting.

3. There are as yet no working undulators based on Nd-Fe-B hybrid magnets; wigglers based on these magnets are presently being constructed.

It will be argued later that very little radiation impinges on the walls of the vacuum chamber of the 6 GeV IDs, and hence the primary concern at present in using Nd-Fe-B undulators is the variation in the ambient temperature. For the purpose of this proposal, we will present design parameters based on REC hybrid magnets. By the time the IDs are built for the present ring, we will have enough experience with Nd-Fe-B to make the final choice of magnet materials. Also, we would like to keep open the option of using newer magnet materials with superior properties.

With regard to undulator design, we should also point out the following:

1. The gap cannot be reduced below a certain minimum value, since there will be a definite aperture size needed for the positron beam. This minimum will also be governed by the length of the straight section, the vacuum requirements, etc. If the undulator is inserted in the vacuum ring, the minimum gap can be about 0.8 cm. However, this makes the undulator design complex and reduces the flexibility of storage ring operation. On the other hand, if the poles of the ID magnets are located outside the vacuum jacket of the straight section, the minimum gap will have to be about 1.0 to 1.2 cm, to include the vacuum chamber wall thickness.

2. As pointed out earlier, there are constraints on the K values that will permit the ID to work as an undulator. For $K > 3$, the positron deflection becomes appreciable and higher-order harmonics become prevalent in

the energy spectrum. The utility of higher harmonics (n > 3) is often limited in undulator applications. The value of K cannot be infinitesimally small either. Any value of K smaller than 0.2 drastically reduces the photons from the device.

For the 6 GeV storage ring, we have calculated the first-harmonic energy E vs G/λ_o for hybrid REC undulators with various values of λ_o. The plots are shown in Fig. 9. The variation of K vs G/λ_o for various values of λ_o is shown in Fig. 10. The boundaries of these figures are determined by the constraints discussed above, viz., $G \geq 0.8$ cm, $0.07 \leq G/\lambda_o \leq 0.7$, and $K \geq 0.2$. These diagrams can be used to define the 6 GeV hybrid REC undulator parameters required to deliver various first- and higher-harmonic energies.

Such plots are also easily generated for the hybrid Nd-Fe-B undulators. For $\lambda_o = 1.6$ cm, the gap required to produce a 20 keV first-harmonic energy with this undulator is about 1.2 cm, versus 1.0 cm for an optimized hybrid REC configuration.

We can also observe from Fig. 9 that the tunability of energy differs for undulators with different periods. It is very limited for the short-period undulators. This will be discussed in more detail in the next section.

7 Undulator Tunability

One can easily obtain photons of different energy at the experimental sample by use of a monochromator, if the spectral distribution is wide and continuous. This is true with both BM and wiggler sources. However, when the spectral distribution is discrete, as in the case of an undulator, detailed thought must be given to the question of energy tunability. At least three tuning procedures can be considered: (1) In Section 5, it was pointed

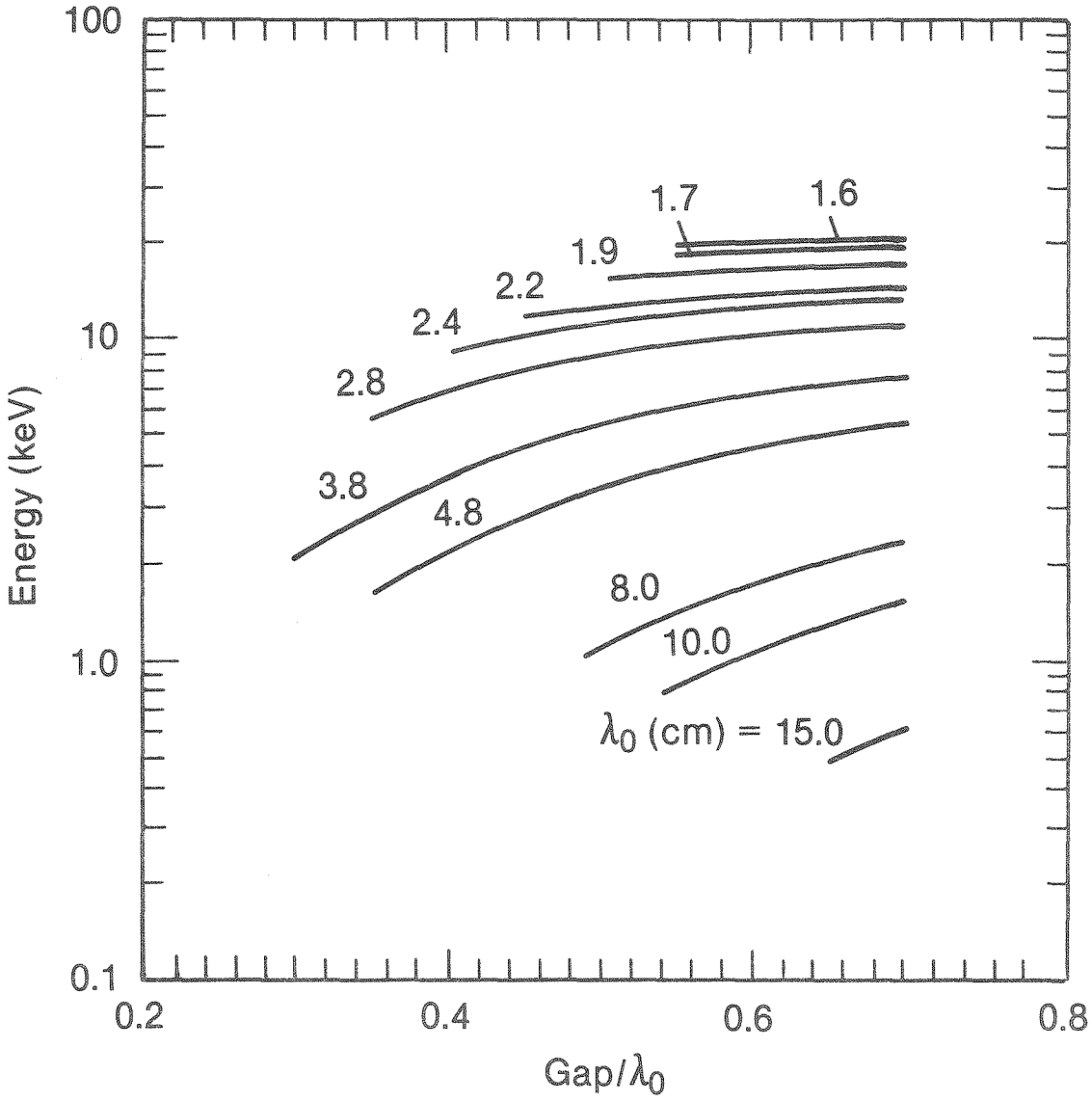

Fig. 9 Energy of radiation as a function of G/λ_o for a set of hybrid undulators with different periods

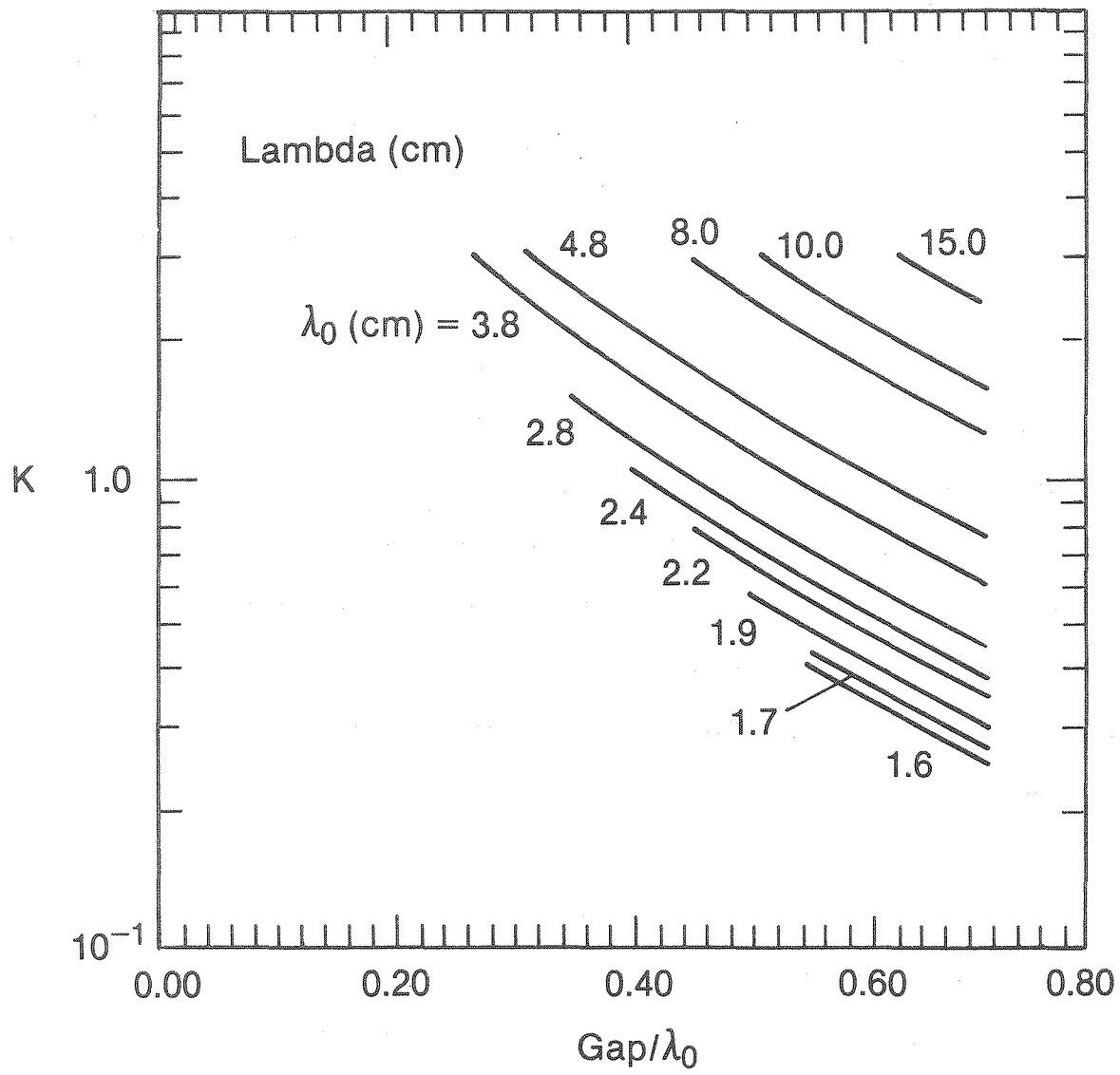

Fig. 10 Deflection parameter K as a function of G/λ_o for a set of hybrid REC undulators with different periods

out that the on-axis undulator peaks have an energy spread of about 4-5%. If the experimental needs are within this range and the change in the spectral intensity over this range can be tolerated, then a monochromator can be used. (2) It is also apparent from Eq. (15) that, by selecting the undulator radiation at different angles with respect to the undulator axis, one can obtain variations in photon energy. (3) As has already been pointed out in the last section (and Table 3), in many cases undulator gap variation will provide the required energy tuning. In this section we will discuss these in some detail.

1. To observe the details of the first-harmonic spectrum, in Fig. 11 we have plotted the flux through a pinhole of 8.5 μrad x 8.5 μrad divergence placed on the axis of the undulator emitting 11 keV radiation (see Table 3, Case A, undulator parameters). Use of a monochromator on such an energy peak provides limited tunability which may be adequate in some investigations. If the dynamic range of the experimental components (optics and detector) is broad enough, even in the valley of the spectral distribution, the brilliance is high enough (higher than the BM sources) to be profitably utilized.

2. It can be seen from Eq. (15) that the undulator peak energy varies with observation angle; this is discussed in detail in Ref. 2. The energy of the photons can hence be changed by merely moving the pinhole away from the undulator axis and using a properly designed monochromator. This of course demands considerable stability of the photon beam, and feedback mechanisms are needed to keep the angular position of the beam stable. Alternative procedures involve the use of sophisticated x-ray optics consisting of a movable mirror-monochromator combination.

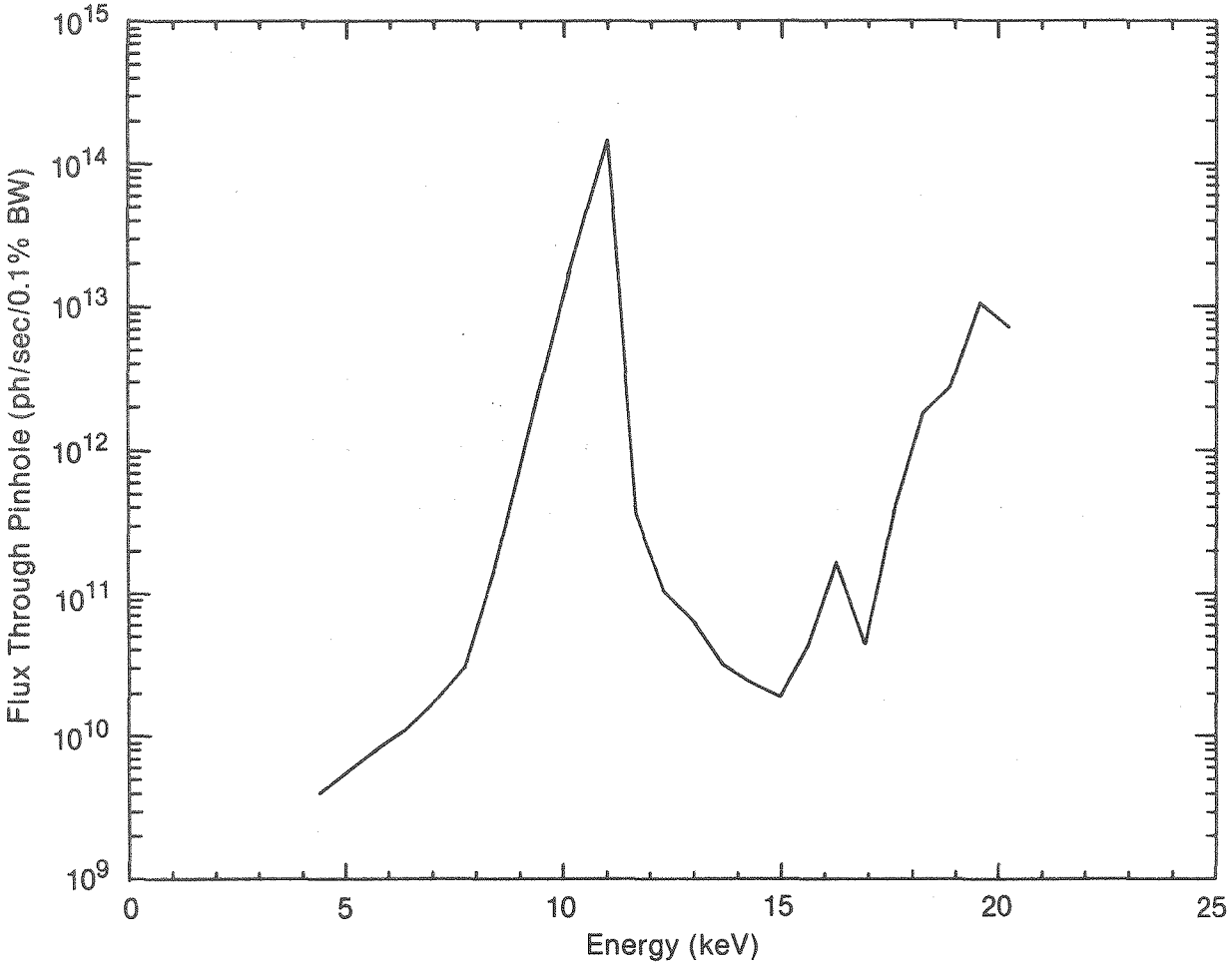

Fig. 11 Flux through a pinhole of 8.5 μrad x 8.5 μrad placed on the axis of an undulator

3. In Fig. 4, we showed the range of tunability that could be achieved for one of the undulators by varying the undulator gap. Table 6 shows the energy-tuning capability, based on gap variation, for a typical set of hybrid undulators designed for the 6 GeV storage ring. This set of 5 m long undulators covers the first-harmonic-energy range from 3.0 to 20 keV. The calculated energy and brilliance values from Table 6 are plotted in Fig. 12, and the analogous values for the third-harmonic radiation are plotted in Fig. 13. The tunability range of the undulators delivering higher first-harmonic energies (#1-#4) can be increased by operation of the storage ring at higher positron energies.

There are numerous questions regarding the undulator energy tuning achieved through gap variation. In the present design of the storage ring, considerable effort has been expended to make the undulator a transparent device with respect to the storage ring. Also, the design includes required beam monitoring and feedback systems, which will reduce the interaction between IDs to a minimum. Hence, it will be possible to vary the gap at one undulator without perturbing the photon beam delivered by other sources on the ring. (As a consequence of this arrangement, gap variation will be possible at only one device at a time.) The task of varying the gap will be handled by the storage-ring operations group. The frequency of gap variation at any device will depend on the operating experience gained at the ring. In the worst-case scenario, the gap variation might have to be carried out prior to a new injection of positrons into the ring. Limited energy variation can be accomplished by a monochromator, as described above.

In both the first- and third-harmonic cases, the tunability of the undulators varies between 5% and 50% of the photon peak energies (see Figs. 12 and 13). If a larger variation of photon energy is desired at a given beam

Table 6

Tunability of Typical 5 m Long Hybrid REC Undulators
for the 6 GeV Storage Ring

Undulator	Undulator Period, λ_o (cm)	Gap, G (cm)		First-Harmonic Energy, E (keV)		Peak Deflection Parameter, K		First-Harmonic Brilliance, BR[a]		Number of Periods, N
		G_1	G_2	E_1	E_2	K_1	K_2	B_1	B_2	
1	1.6	0.92	0.78	20.0	19.0	0.37	0.50	1.2	2.1	312
2	1.7	1.22	0.82	19.5	17.5	0.25	0.54	0.5	2.3	294
3	1.9	1.44	0.90	17.5	15.0	0.25	0.63	0.5	2.5	263
4	2.2	1.72	1.06	15.0	12.5	0.27	0.70	0.5	2.5	227
5	2.4	2.03	1.16	14.0	11.0	0.25	0.77	0.4	2.4	208
6	2.8	2.56	1.39	12.0	9.0	0.25	0.85	0.3	2.4	178
7	3.8	3.47	1.80	8.5	5.0	0.34	1.26	0.4	2.5	131
8	4.8	4.33	2.22	6.5	3.0	0.44	1.66	0.5	2.2	104

[a]On-axis value, in ph/sec/0.1%BW/mrad^2/mm^2.

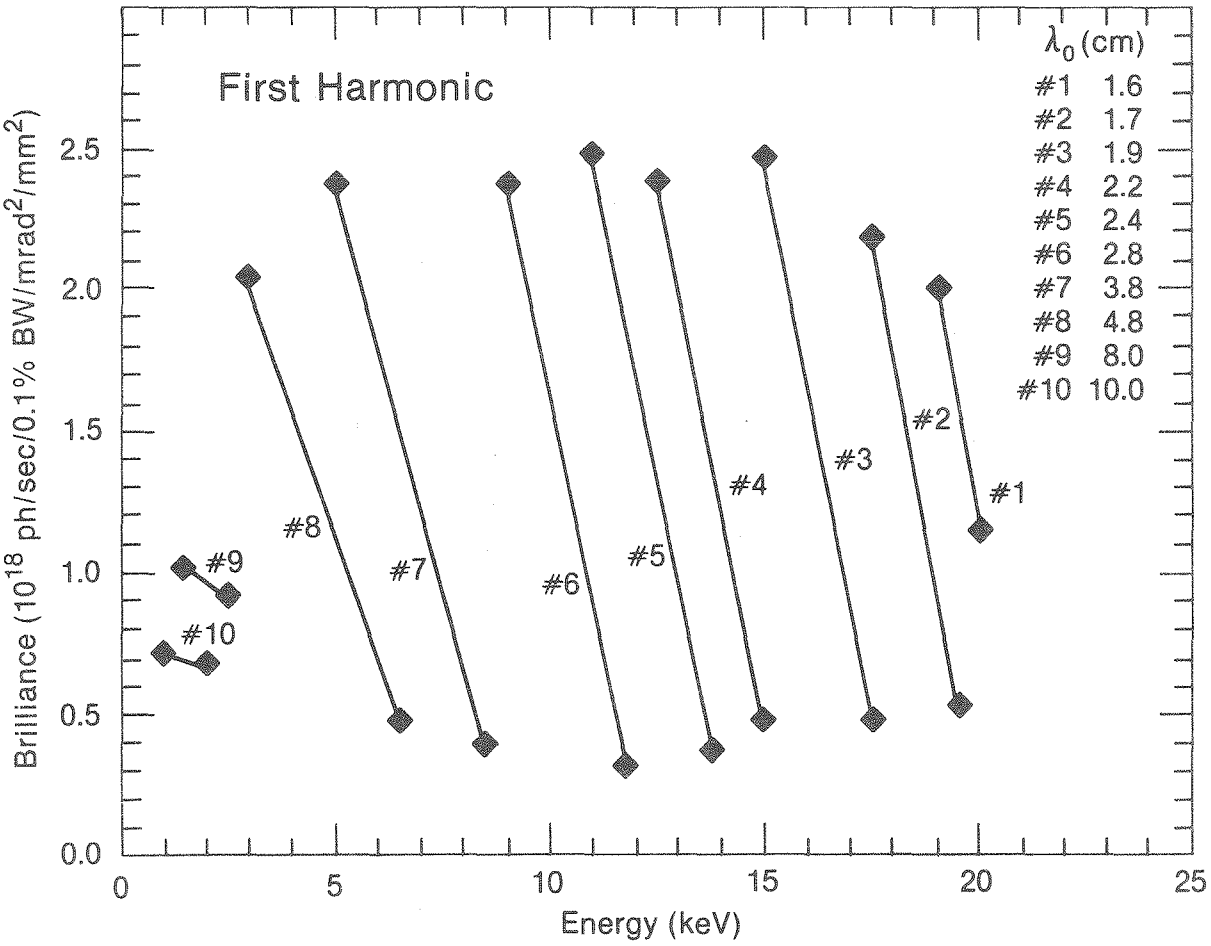

Fig. 12 First-harmonic energies available with variable-gap undulators with periods between 1.6 and 10 cm

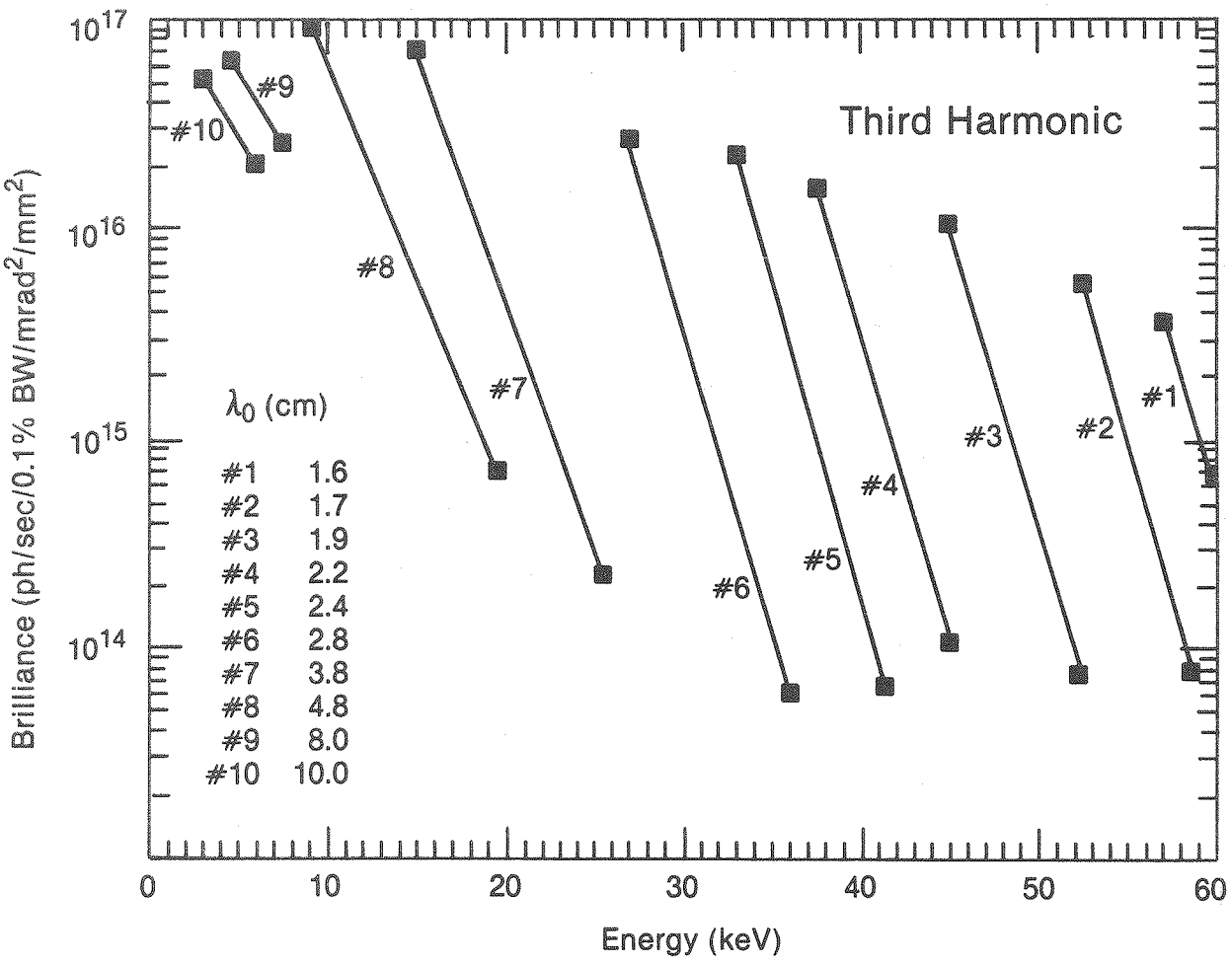

Fig. 13 Same as Fig. 12 for the third-harmonic energy

port, then the experimenter should use either the radiation in the higher harmonic range at the cost of peak brilliance (depending on the K value of the device) or a set of undulators with different first-harmonic energies, assembled at a single straight section on a carousel. Switching of undulators on a carousel will have to be done less frequently than gap variation.

Procedures will be established to accomplish either the gap variation or the device switching at a straight section through the use of software locks at various levels of sophistication, as needed. This will ensure successful and smooth operation of the storage ring without interaction between various experiments.

In summary, undulator energy tuning, by means of either a gap variation or device switching, is desirable at a 6 GeV storage ring; with a properly structured procedure, this can be accomplished by the storage-ring operations group after implementation of the essential diagnostics and monitoring that are included in the present design.

8 Insertion Device Vacuum Chambers

In choosing the design of the vacuum chamber in the straight sections, the following points are to be considered:

1. The vacuum enclosure will be all metal for maintenance of a low outgassing rate and for resistance to radiation and heat (either from the radiation or from baking).

2. The internal profile of the vacuum chamber should be smooth and continuous to minimize beam-induced heating.

3. The vertical aperture of the chamber should be such that injection of the positron beam can be achieved without any beam loss. The minimum

desirable magnet gap for an undulator with first-harmonic energy of 18-20 keV is of the order of 1.0 cm. This gap is a sum of the vertical aperture and the wall thicknesses of the chamber. If a larger gap is feasible, the vertical aperture should be commensurately larger.

4. The wall thickness should be adequate to take the mechanical stresses from the vacuum inside the chamber and from any heating that occurs (from radiation or from baking).

5. The design should allow attachment of pumps such that the required low vacuum can be easily achieved. The average pressure P_{av} in a straight section of length L (in cm) with n symmetrically placed pumps, each of speed S (in ℓ/sec), is

$$P_{av} = \frac{qbL}{Sn} + \frac{qbL^2}{12Cn^2} , \qquad (21)$$

where q = specific outgassing rate (usually $<10^{-11}$ torr·ℓ/sec/cm^2),

b = peripheral length of the inner section of the chamber (cm),

C = specific conductance constant (ℓ·cm/sec)

6. The chamber material should have low magnetic permeability even after metal working and baking.

In view of the above considerations, the final selection of the ID vacuum chamber is contingent on the gap requirements of the IDs. At this time, we have considered three vacuum chamber geometries that will meet most of the needs of the IDs. They are discussed in some detail below.

Type A vacuum chamber: This is a rigid vacuum chamber with a maximum vertical aperture of 16 mm and a minimum wall thickness of 2 mm, which will provide a minimum ID gap of 2.0 cm. A schematic cross section is shown

in Fig. 14a. Such a chamber would be suitable for many IDs. For example, let us consider a wiggler with a 20 cm period. The minimum value of G/λ_o will be 0.1 in this case. If a hybrid REC configuration is used, one can achieve values of B_o = 1.85 T and K = 35. We could also consider a whole set of undulators built around such a vacuum chamber, which can deliver first-harmonic radiation with energy as high as 14 keV (see Table 6).

The average pressure in a Type A ID vacuum chamber, 6 m long, can be calculated from Eq. (21). With b = 16 cm and C = 1010 ℓ·cm/sec for nitrogen, P_{av} = 1.3 x 10^{-9} Torr can be achieved with two symmetrically placed pumps with a speed of 100 ℓ/sec. In this calculation we have assumed the outgassing rate to be 10^{-11} Torr·ℓ/sec/cm^2. This is a typical rate for a baked metal chamber. However, the photodesorption will increase the outgassing at initial stages of the ring operation.

The vacuum chamber aperture in any plane should be large enough to result in a long positron-beam lifetime and should allow for closed-orbit errors. The required aperture δi can be estimated as follows:

$$\delta i = \pm \left[(\text{closed-orbit error}) + 10\ \sigma_i\right],\ i=x,y. \qquad (22)$$

The value of σ can be estimated, for the worst-case scenario of full coupling, to be 0.2 mm for the present lattice design. Assuming the vertical closed-orbit error to be 2 mm, we obtain $\delta y = \pm 4$ mm. With a larger closed-orbit error of 10 mm in the horizontal direction, the estimated minimum horizontal aperture needed will be $\delta x = \pm 12$ mm. Since the positrons are injected in the horizontal plane in this design, we should add a 12 mm allowance to δx for injection. Hence, $\delta x = \pm 24$ mm.

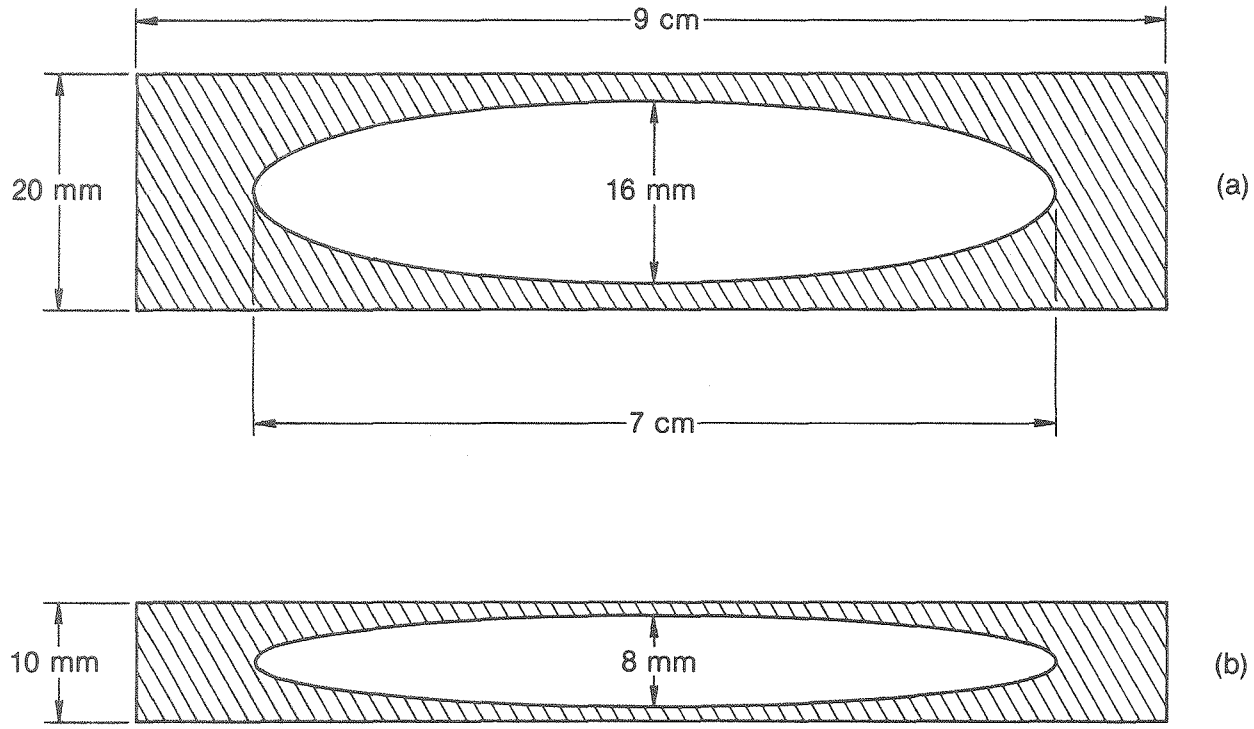

Fig. 14 Cross section of two ID vacuum chambers with different apertures

In summary, the type A vacuum chamber is suitable for most of the straight sections and meets all the requirements for successful machine operation.

Type B vacuum chamber: This chamber is similar to type A, except that the vertical aperture is 8 mm and the minimum wall thickness is 1 mm. (See Fig. 14b). The minimum ID gap with this vacuum chamber is 1.0 cm. Thus this chamber is suitable for undulators needing small gaps, like the one capable of delivering 20 keV first-harmonic radiation (#1 in Table 6). The calculations indicate that the walls of this chamber have adequate mechanical integrity. However, the body of the chamber can be ribbed to increase the mechanical strength. In this case, the structure of the rib will have to be matched with the undulator period.

The average pressure in this vacuum chamber can be as low as that for the type A chamber. The vertical aperture, on the other hand, is just adequate for successful injection (as discussed above for the type A chamber). Hence we recommend that experience be acquired in reducing closed-orbit errors before this chamber is used for undulators where small gaps are needed. If there are problems with injection in the small aperture of the rigid chamber, we suggest a movable vacuum chamber with an adjustable aperture, as discussed below.

Type C vacuum chamber: Unlike the previous two types of vacuum chambers, this one permits enlargement of the aperture as needed during the injection. The aperture can subsequently be reduced so that very small gaps can be achieved. Such a vacuum chamber has been successfully operated at SSRL on the 54-pole wiggler beamline. A drawing of this chamber is shown in Fig. 15. The flexibility in the chamber aperture is provided by the omega joints and racetrack plan; one can obtain a maximum aperture of 1.8 cm, which is

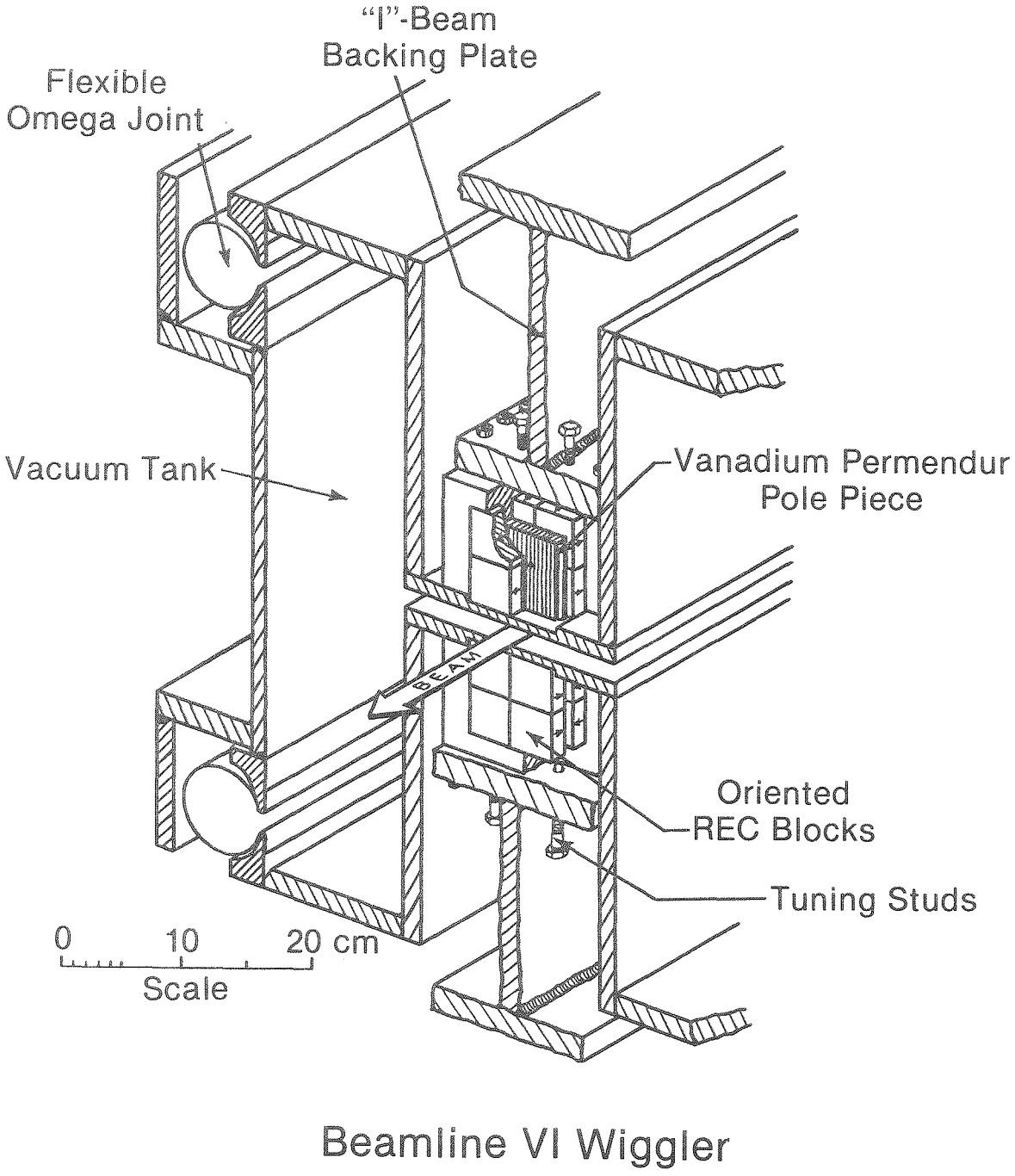

Fig. 15 A flexible vacuum chamber suitable for the 6 GeV IDs (drawings XBL 833-8953, courtesy of Lawrence Berkeley Laboratory)

suitable for positron injection in our lattice design. When the omega joints are closed, the ribbed body design permits a minimum gap of 0.8 cm. The undulator magnet stack is moved independently of the omega joint motion, so that the chamber provides great flexibility for gap adjustments. The pumping needs for such a vacuum chamber can be met with a pump speed of 1500 to 2000 ℓ/sec.

Although this vacuum chamber is ideal for small-gap ID applications and has already been designed for shorter ID lengths, it is complex in detail compared to a rigid type B vacuum chamber. The mechanical tolerances for longer vacuum chambers are bound to be more stringent, and this should be an important factor in the final choice of the design.

In summary, it is advisable to use type A vacuum chambers for straight sections in the initial period of storage ring operation. When enough experience has been gained in injection, one could select either of the low-gap vacuum chambers (type B or type C), depending on the application. Use of Nd-Fe-B rather than REC hybrid magnets will relax the minimum gap requirements by about 2 to 4 mm, depending on the ID. This will work very favorably in designing type B chambers with larger apertures to facilitate injection.

9 Undulator Design Tolerances

The design parameters of an undulator can be selected on the basis of the considerations outlined above. All aspects of the technical and engineering design need careful consideration. These include a spread in λ_o along the length of an undulator, non-ideal field distribution, non-uniform gap, etc.

Inhomogeneity of the field will be detrimental to the production of high brilliance. Such variations in the field, ΔB_o, will broaden the undulator peak:

$$\frac{\Delta E_n}{E_n} = \frac{K^2}{1 + K^2/2} \frac{dK}{K} = \frac{K^2}{1 + K^2/2} \frac{\Delta B_o}{B_o} . \qquad (23)$$

The pole pieces have to be chosen with care to ensure well-matched magnet pairs, which will reduce ΔB_o. Careful assembly of the magnets is also crucial to the proper definition of the positron trajectory. Hence, the field distributions will have to be measured after all the pole pieces are assembled. Integral field measurements should be carried out to make sure that the field integral is zero over each half of the undulator for all field levels (various gaps). Specifically desi;vrmx mix›fconk ¶ino"ermri"evrnib›cc electromagnets) are needed for nulling the field integral W

Even if the pole pieces are selected with great care and are assembled to form a "perfect" undulator to reduce ΔB_o, the misalignment of the undulator axis with respect to the positron trajectory will destroy the vertical field homogeneity. ΔB_o is a function of vertical misalignment and the undulator period. The extent of the field aberration will be greater in small-period undulators with small gaps. This aberration is hence related to the tolerance of the vacuum chamber geometry along its length.

In summary, the undulator designs should aim for minimum field errors, and these should be measured at every stage of undulator assembly and installation. It is obvious from the discussions of the last two sections that there is not much demand for undulator harmonics higher than the third. The tolerance requirements for the first few harmonics are less stringent in our lattice because of the intrinsic energy broadening (discussed in Section

5) due to positron beam divergence.

From the detailed measurements of field errors carried out by Spectra Technology on the 54-pole device (λ_o = 7 cm) built by Lawrence Berkeley Laboratory and on a high-precision 5 m long undulator (λ_o = 2.18 cm, 450 poles), it is estimated that even for the shortest-period undulator planned for the present 6 GeV lattice, a field error of less than 0.5% can be achieved. It is easy to hold the error below this value for the longer-period devices.

The field errors can also influence the synchrotron tune shift. The horizontal tune shift $\Delta\nu_x$ can be estimated from the relation

$$\Delta\nu_x = \frac{\Delta B\ \beta_x \lambda_o \sqrt{N}}{4\sqrt{2}\pi B_o \rho}\ , \tag{24}$$

where ρ is the radius of the positron trajectory in the undulator. For λ_o = 2 cm, $B_o\rho$ = 200.1 kG•m, β_x = 20 m, N = 200, and B_o = 3000 G, a field error of 0.5% results in a horizontal tune shift of 2.4×10^{-3}. This should not hinder the successful operation of the storage ring.

Another important tolerance factor concerns the bend angle in the positron trajectory along the undulator. For successful operation of the undulator, the cumulative error in the bend angle due to the field error ΔB_o should not greatly exceed the beam divergence. The cumulative bend-angle error is given by

$$\Delta\theta = \lambda_o \sqrt{N}\ \Delta B_o / (\sqrt{2}\ B_o \rho). \tag{25}$$

The value of $\Delta\theta$ in the above example would be 15 μrad. This is comparable to the positron beam divergence in the lattice design in an undulator straight

section. Thus the field error of 0.5% is, in general, acceptable for meeting the various tolerance criteria we have discussed.

10 Angular Distribution of Power from Various Sources

When one delivers a very brilliant photon beam, one also delivers a large amount of radiated power concentrated in an extremely small solid angle from the low-emittance 6 GeV storage ring. This power will have to be handled in a beamline by various components such as absorbers, masks, filters, pinholes, windows, and the optical elements (mirrors and monochromator crystals). In this section, we present a quantitative evaluation of the radiated power from the various sources and their angular dependences.

10.1 Bending Magnet Sources

The angular dependence of the power emitted by a BM, in units of W/mrad θ/mrad ψ, is given by

$$\partial^2 P/\delta\psi\delta\theta = 1.24\times10^{-2} E_R^{\,4} B\ I\ S(\gamma\psi), \tag{26}$$

where E_R is in GeV, B is in T, I is in mA, and

$$S(\gamma\psi) = (1 + \gamma^2\psi^2)^{-5/2}\ [7 + 5(\gamma^2\psi^2)/(1 + \gamma^2\psi^2)]/16. \tag{27}$$

The distribution is shown in Fig. 16, where the total power is represented by the area under a rectangle of width equal to 2 x 0.77/γ. The peak power of this distribution (ψ = 0), in W/mrad θ/mrad ψ, is

$$\delta^2 P/\delta\psi\delta\theta(\psi=0) = 5.4\ \times\ 10^{-3}\ E_R^{\,4} B\ I. \tag{28}$$

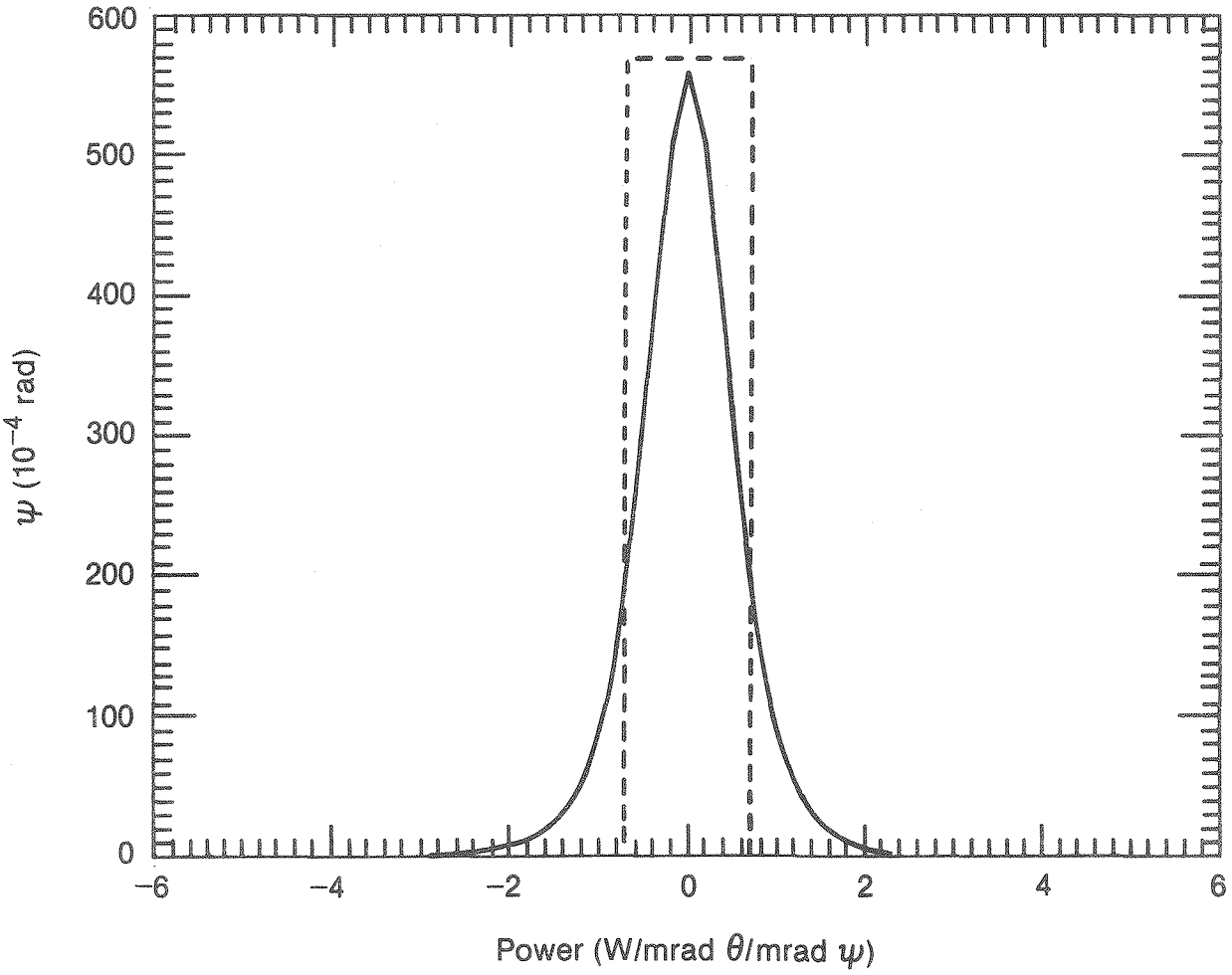

Fig. 16 Power distribution of radiation from a BM on a 6 GeV storage ring as a function of vertical opening angle ψ

For the design considered here (B = 0.8 T, E_R = 6 GeV, and I = 100 mA), the peak power density is 560 W/mrad θ/mrad ψ.

By integrating for all θ and ψ, we obtain the total radiated power (in watts) from a BM:

$$P = 1.263\ E_R^2 B^2 I\ L, \tag{29}$$

where L (= 2.45 m) is the length of the positron trajectory through the BM. For our lattice, P = 7129 W. Thus, per mrad θ, the radiation provides 73 W of average power over all ψ. In Table 7, we contrast the power distribution from the BMs at NSLS and the present 6 GeV lattice. The peak power density delivered by the present lattice is considerably larger than that from NSLS, whereas the total power does not show the same increase.

Table 7

Comparison of Power Delivered by Two BM Sources

	6 GeV	NSLS
E (GeV)	6.0	2.5
I (mA)	100	500
B (T)	0.80	1.22
ρ (m)	25.0	6.8
E_c (keV)	19.2	5.1
2ψ (mrad)	0.17	0.41
Average Power (W/mrad θ)	73	40
Peak Power (W/mrad θ/mrad ψ)	560	128

10.2 Insertion Device Sources

The total power (in watts) radiated from an ID of length L (in meters) is given by

$$P = 0.633\ E_R^2\ B_o^2\ I\ L, \tag{30}$$

where B_o is the peak field in the ID. The angular dependence of this power (in W/mrad θ/mrad ψ) is

$$\delta^2 P/\delta\theta\psi = 0.01084\ E_R^4\ B_o I\ N\ G(K)\ f_K(\theta,\psi), \tag{31}$$

where N is the number of periods in the ID and K is the usual deflection parameter. In the above,

$$G(K) = (K^7 + 24K^5/7 + 4K^3 + 16K/7)/(1 + K^2)^{3.5} \tag{32}$$

and $f_K(\theta,\psi)$ is a complex integral normalized to 1. For $\psi = 0$ and $\theta = 0$, the peak power density (in W/mrad θ/mrad ψ) is obtained from

$$\delta^2 P/\delta\theta\delta\psi\ (\theta=0,\psi=0) = 0.01084\ E_R^4 B_o I\ N\ G(K). \tag{33}$$

It is important to note from Eq. (32) that much of the variation in G(K) is for K values smaller than 1.0, with G(K=1.0) = 0.94. As we approach the wiggler regime (K ≫ 10), the value of G(K) approaches 1; G(∞) = 1.0. Hence the variation in the peak power density for a given undulator increases as K approaches 1.0 and then saturates for larger values of K.

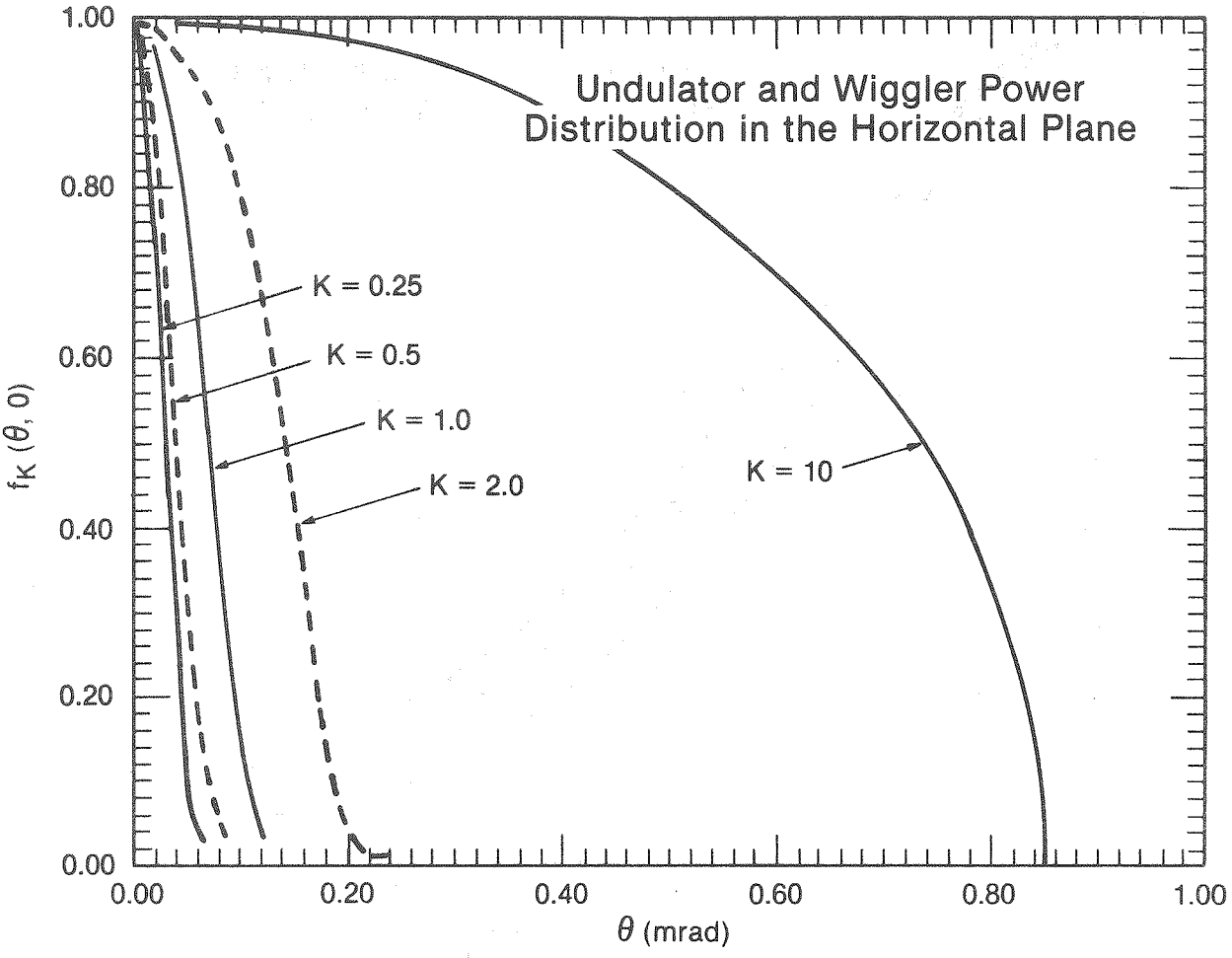

Fig. 17 The horizontal section of the power distribution $f_K(\theta,0)$ for IDs with various K values

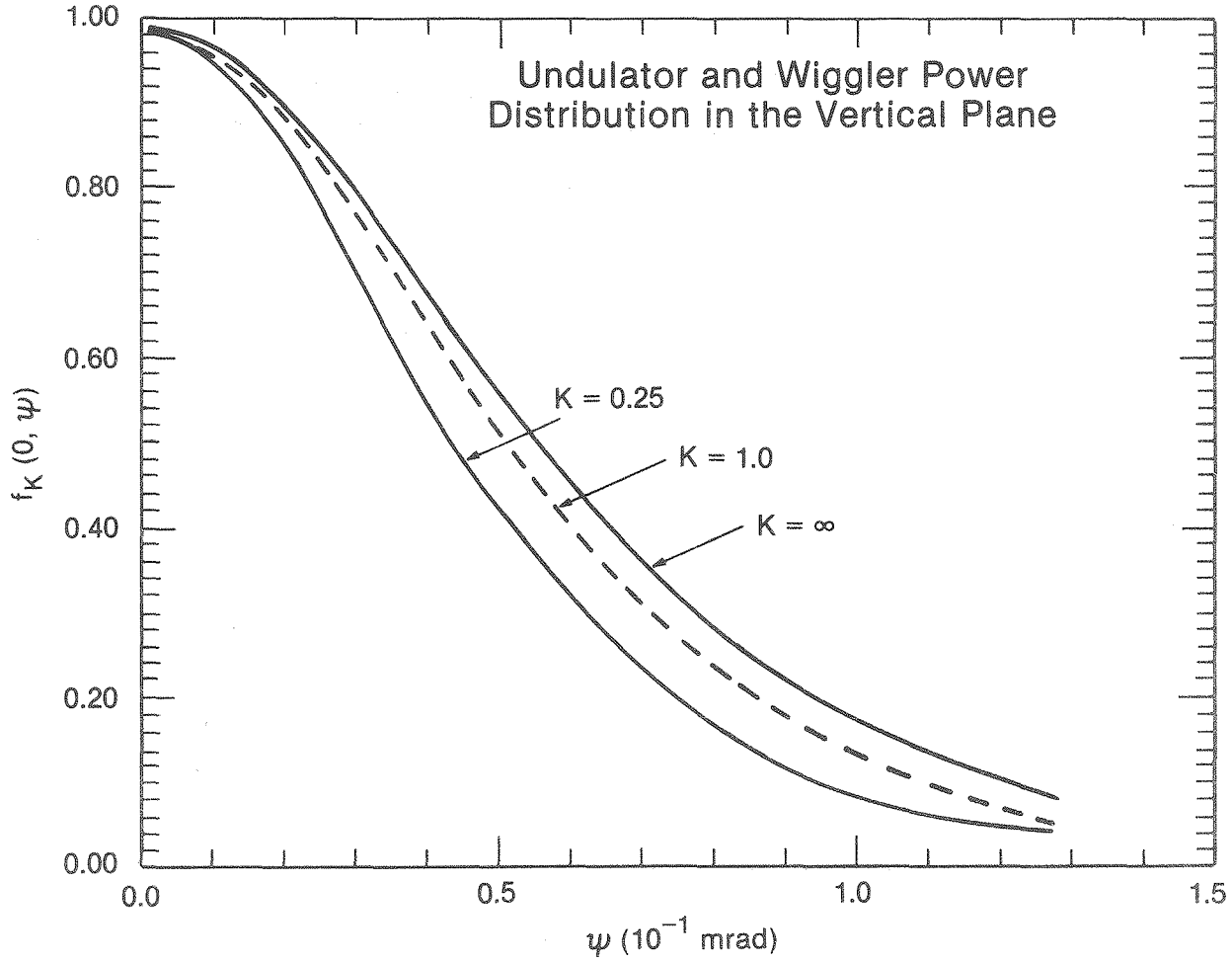

Fig. 18 The vertical section of the power distribution $f_K(0,\psi)$ for IDs with various K values

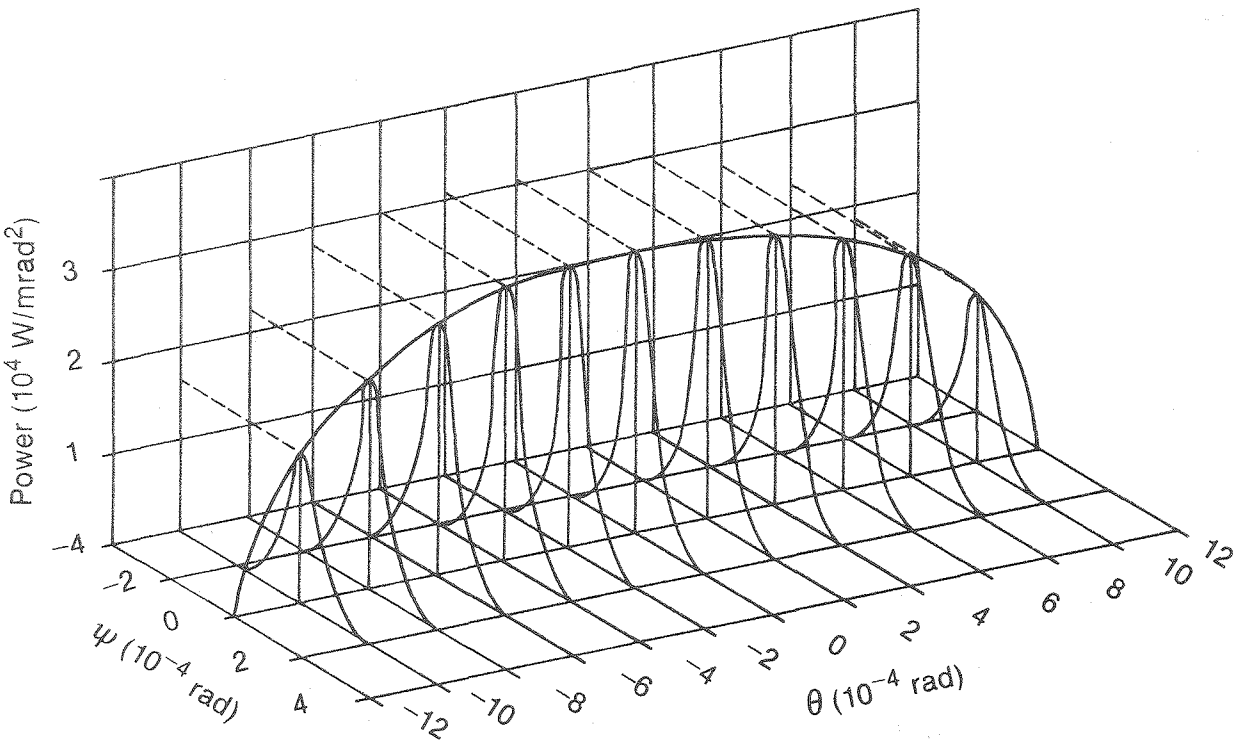

Fig. 19 Distribution of power along ψ and θ for radiation from a 1.5-T, 15-period wiggler on a 6 GeV storage ring (100 mA)

The horizontal and vertical sections of the angular power distribution for 6 GeV IDs with various values of K, namely $f_K(\theta,0)$ and $f_K(0,\psi)$, are shown in Figs. 17 and 18, respectively. It should be pointed out that the vertical distribution for $K = \infty$ is identical with that of a BM, as given by Eq. (26). Thus the extent of the vertical distribution of radiation power from any real ID will be smaller than that from a BM. The horizontal power distribution, $f_K(\theta,0)$, approaches that of a wiggler as K increases, with the power cutoff at $\pm K/\gamma$. The extent of horizontal distribution of the power density for a typical undulator is always smaller than that for a wiggler and increases with increasing K.

Let us consider a typical hybrid REC undulator with $\lambda_o = 1.9$ cm, for which the first-harmonic energy is ~15 keV. For this undulator, L = 5 m, N = 263, $B_o = 0.35$ T, $\lambda_o = 0.9$ cm, and K = 0.63. From previous equations, it is found that the total power radiated by this device is 1395 W, and the peak power density is 113 kW/mrad^2. Most of the radiated power is distributed in a solid angle of approximately 130 x 130 μrad^2. Next let us consider a wiggler on the 6 GeV ring with $B_o = 1.5$ T, N = 15, $\lambda_o = 10$ cm, and K = 14. The total power from this wiggler is 7.67 kW and the peak power density is 31.6 kW/mrad^2. The horizontal power distribution spreads between ± 1.2 mrad. The envelope from the angular distribution of the power density for this wiggler is shown in Fig. 19.

Often it is more useful to consider the power distribution on a surface located D meters away from the center of the ID. The normal radiation impinging on a surface can be defined by peak surface power density W_{xy} (in W/mm^2):

$$W_{xy} = [\delta^2 P/\delta\theta\delta\psi \text{ (at } \theta=0,\ \psi=0)]/\ D^2. \qquad (34)$$

In the above undulator and wiggler examples, the values of W_{xy} at a distance of D = 20 m from the source are 282 and 79 W/mm^2, respectively. This power falls off rather fast as we move away from the axis of the ID in both the x and y directions. At normal incidence, the power from the undulator exposes an area of roughly 2.6 mm x 2.6 mm at a distance of 20 m. The analogous area for the wiggler is 3 mm x 24 mm.

The above understanding of the angular distribution of radiation from IDs on the 6 GeV storage ring has the following important consequences: Negligible amounts of radiation from the IDs will strike the walls of the vacuum chamber even when the chamber aperture is 8 mm (type B chamber). Thus the photodesorption from the walls of the IDs is not significant. Also, no cooling of the ID walls is necessary. The magnetic structure will not be exposed to the radiation. Hence there will be no radiation degradation of the magnetic properties that are otherwise anticipated, nor will the magnetic structure be heated by the radiation. Also, the extraction of the radiation from the ID should be simple, and no extra shielding will be needed in the vicinity of the radiation ports. However, the ID radiation will pass through the fringing field of the next BM. This will contaminate the ID radiation with soft x-ray radiation. This will be of consequence only in low-energy undulators, if at all.

11 Polarization of Radiation from Various Sources

In many experiments, the polarization characteristics of the radiation are of paramount importance, and synchrotron sources provide many possibilities for obtaining radiation of the desired polarization.

11.1 Polarization from BM and Wiggler Sources

The radiation from BM sources is linearly polarized in the orbital (xz) plane. The critical energy radiation (19.13 keV) from our lattice is 99.92% linearly polarized. With increasing ψ, the perpendicular polarization gradually increases at the cost of polarization parallel to the xz plane. These two components of polarization are phase correlated, and hence one can obtain elliptically polarized radiation as ψ increases. The polarizations above and below the xz plane are opposite in helicity. The ellipticity of the radiation at any given angle also depends on the energy of the radiation.

On passing through a transverse multipole wiggler, the positron beam experiences bending forces in two opposite directions. Hence, the radiation is linearly polarized only in the orbital plane (xz). Away from this plane, polarizations of opposite helicity from successive poles add to destroy the net polarization, except for a residual linear component. This should be contrasted with the situation for a BM or a single-period energy-shifter wiggler.

In some situations, linear polarization in the yz plane rather than in the xz plane is desired. This can be accomplished by designing a multipole wiggler with the positron trajectory in the yz plane (and the field along the xz plane). The difficulty in such a design arises from the need to have a larger gap in order to accommodate a large aperture for the ID vacuum chamber in the xz plane. In spite of this, a wiggler can be designed by using permanent magnets with the field in the xz plane (see Ref. 2).

A helical wiggler can deliver radiation with circular polarization along the axis of the device. However, such a device will produce strong coupling between the horizontal and the vertical motion, with a resultant

increase in vertical beam size. Hence, we shall not consider such a device for the present lattice at this time.

11.2 Polarization from Undulator Sources

The nature of polarization emitted by a transverse undulator is dependent on the observation angle. The inclusion of the positron beam divergence smears the polarization content of the radiation, but in our design it is not destroyed. Along the x axis one has linear polarization (σ-component), whereas along the y-axis the σ- and π-components appear at various observation angles (see Fig. 20). Our calculations suggest the possibility of selecting a wide variety of ellipticities of polarization by choosing an appropriate observation angle for a given photon energy.

There are two distinct types of undulators which can in principle deliver on-axis radiation with arbitrary polarized radiation. The first one is a helical undulator which delivers circular polarization along the axis. This device presents the same difficulties in its implementation as the helical wiggler discussed above. The second device, which has been proposed by scientists at the Lawrence Berkeley Laboratory, is called a "crossed-undulator." This consists of a set of two orthogonal transverse undulators and can produce polarized radiation of varying ellipticity. It can deliver radiation that is linearly polarized along either the x or the y axis. The design of such a device will demand a vacuum chamber that provides both an acceptable aperture and an appropriate magnet gap in both the x and y directions. This device will need considerable developmental work before it is constructed for the present storage ring.

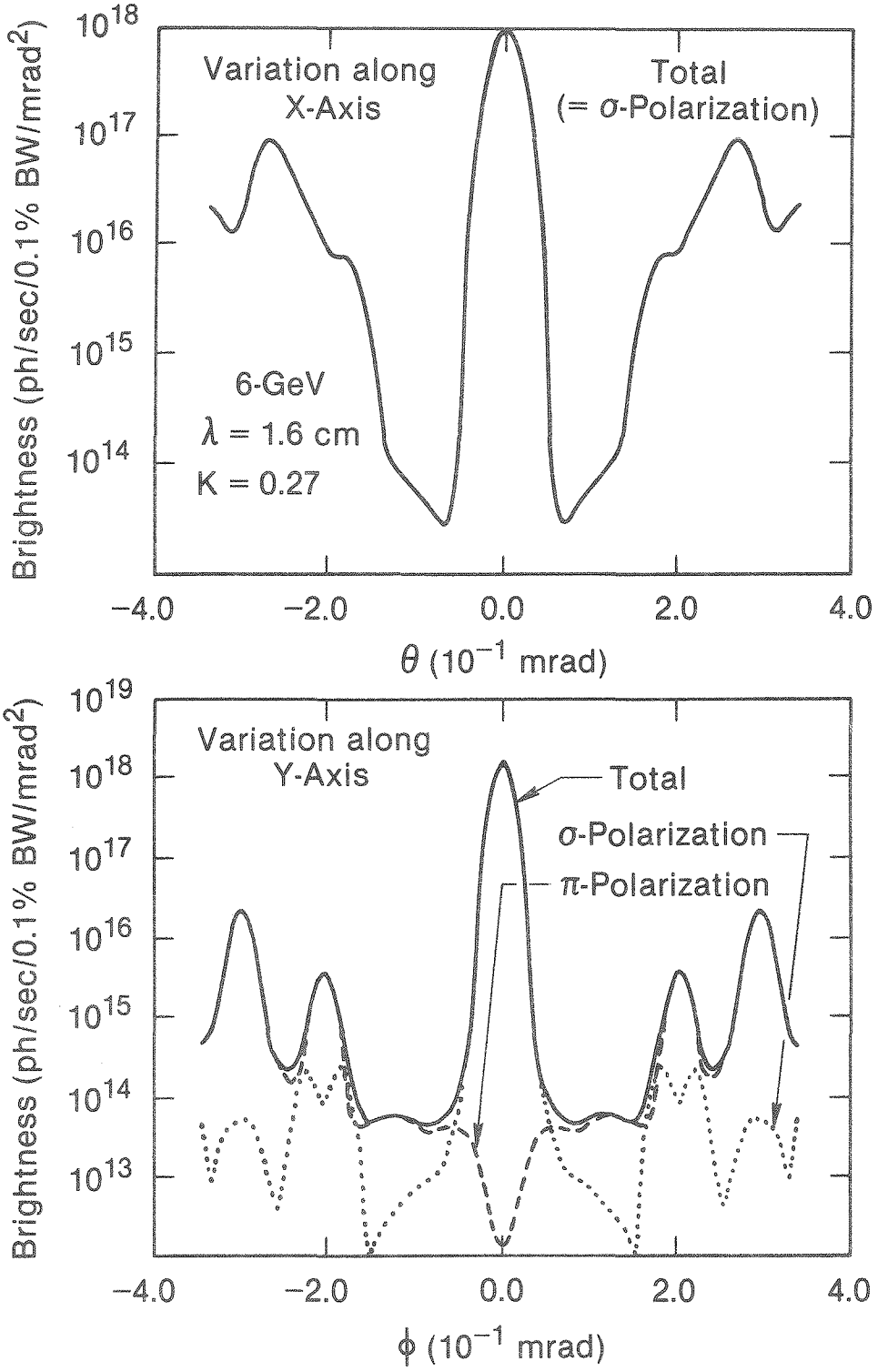

Fig. 20 Angular distribution of 20 keV radiation from a 6 GeV (100 mA) undulator along the x- and y-axes. The σ- and π-polarization components along the y-axis are shown. These calculations include the source size.

12 A 20 KeV Undulator

12.1 Introduction

One of the requirements of the present design is to deliver approximately 20 keV radiation in the first harmonic of an undulator. This design goal was set because a host of scientific experiments in the future will undoubtedly need high-energy, high-brilliance radiation. These range from absorption spectroscopy of the Mo K-edge for understanding the structure of proteins and catalysts to ultrahigh-energy-resolution inelastic scattering from phonons. In this section, we present a preliminary design study on such an undulator.

12.2 Preliminary Design Parameters

Figure 21 shows a schematic layout of the magnetic structure of this transverse undulator. In this hybrid configuration, the magnetic field strength and distribution depend on the geometry of the pole-tips, so that the field quality is much less dependent on the magnetic and geometric quality of permanent magnets. The magnet material could either be REC or Nd-Fe-B for this hybrid geometry. The peak field can be tuned by varying the flux shunts at each pole (see Fig. 21). We have considered two possible materials for the pole-tips: vanadium-permendur and 1010 steel. The design of this device is based on a preliminary optimization of the magnetic structure. In this procedure, various geometrical parameters of the structure were iteratively optimized through a two-dimensional field computation (in the yz plane). The resulting parameters are presented in Table 8. Three-dimensional effects were then roughly estimated to obtain a pole width and magnet width that would not alter the field homogeneity.

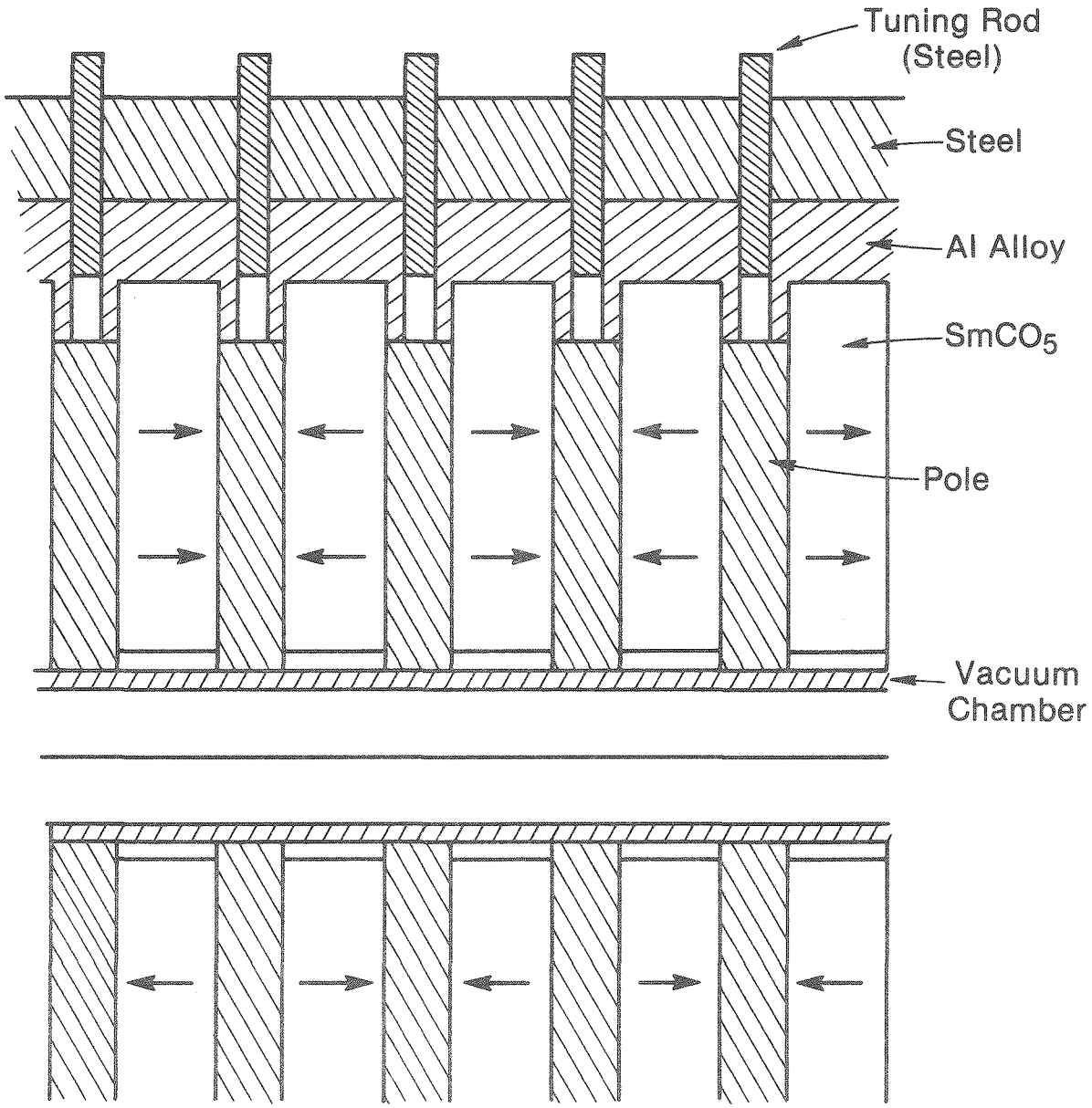

A Hybrid Undulator Configuration

Fig. 21 Hybrid REC geometry selected for the 20 keV undulator. The tuning rods are movable

Table 8

Optimized Parameters of a 20 keV Hybrid REC Undulator

	Parameter
Undulator Period, λ_o (cm)	1.6
Magnet Gap, G (cm)	1.0
Pole Width in x Direction	4.0
Pole Height in y Direction	2.50
Pole Thickness in z Direction	0.45
Magnet Width in x Direction	4.8
Magnet Height in y Direction	3.05
Magnet Thickness in z Direction	0.575
Pole-Tip Overhang in y Direction	0.05
Peak Field On Axis, B_o (T)	0.2356
Peak K On Axis	0.352
Peak Field Increase (%) at 0.1 cm Off Axis in y Direction	3.0
Peak Field Increase (%) at 0.2 cm Off Axis in y Direction	12.0
Decrease (%) Achieved in B_o by Increasing Pole-Tip Overhang to 0.1 cm	5.5
Length of Straight Section (m)	6.0
Minimum Length of Transition Section (m)	0.4
Maximum Length Available for Undulator (m)	5.2
Maximum Undulator Periods Used in Spectral Calculations, N	312

Figure 22 shows the optimized two-dimensional magnetic flux configuration of a half period of the undulator. In arriving at the peak field of 0.2356 T, a residual induction of 0.90 T and a demagnetization force of 8.85 kOe have been used. Use of 1010 steel instead of vanadium permendur for the pole-tips would reduce the peak field by 1.1%. An increase of 1.0 cm in the heights of the permanent magnet and the steel pole increases the peak field by 3% in this optimization.

Figure 23 shows the calculated variation of the y-component of the magnetic field, which almost exactly follows the desired profile along the z-axis, $B_y = B_o \cos 2\pi z/\lambda_o$. Such behavior of the undulator field profile is required in order to predict the radiation spectra from this device. As the trajectory of the positrons is moved 1 mm above the undulator axis, the beam will experience a 3% increase in the peak magnetic field and a field profile that deviates from a cosine function. This deviation is even greater when the trajectory is 0.2 cm above the undulator axis in the yz plane (see Fig. 23).

Figure 24 shows the angle-integrated on-axis spectral brilliance in the vicinity of the first harmonic located at 20.10 keV, for the expected K value of 0.352. If the magnet material is replaced by Nd-Fe-B in the design under discussion, the expected peak field is 0.288 T and the value of K is 0.43. This enhances the first-harmonic brilliance, as shown in Fig. 24. On the other hand, if K = 0.35 is adequate with the Nd-Fe-B configuration, the gap can be increased to 1.1 cm.

12.3 Undulator Vacuum Chamber

We have discussed the vacuum chamber geometries in a general way in Section 8. For an undulator, we have the option of selecting a flexible type C chamber based on omega joints and a racetrack plan (Fig. 15) or a rigid type

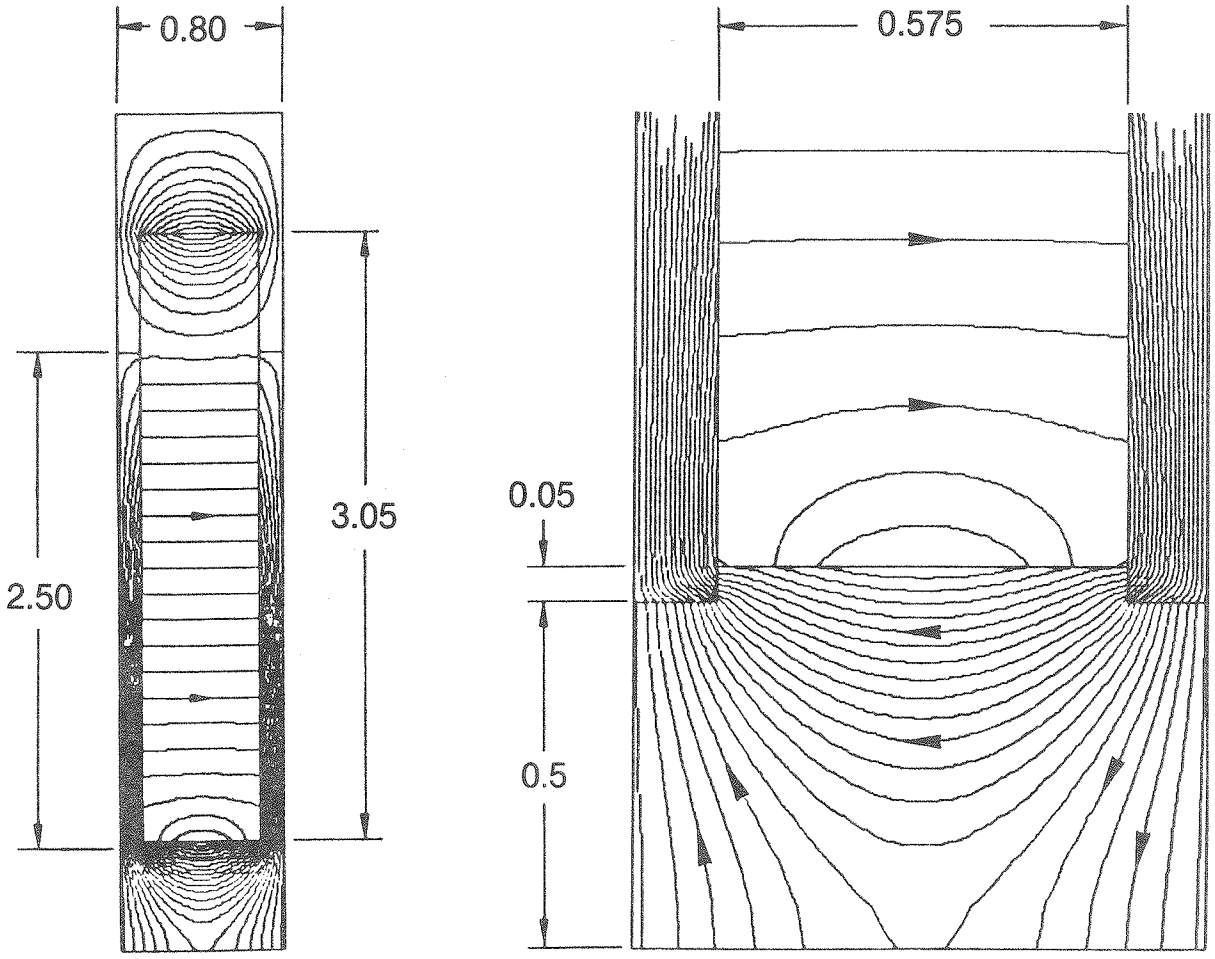

Fig. 22 Magnetic flux profile of a half-period of a 20-keV hybrid REC undulator (λ_o=1.6 cm). Dimensions are in cm. The drawing on the right show a detail of the pole overhand discussed in the text.

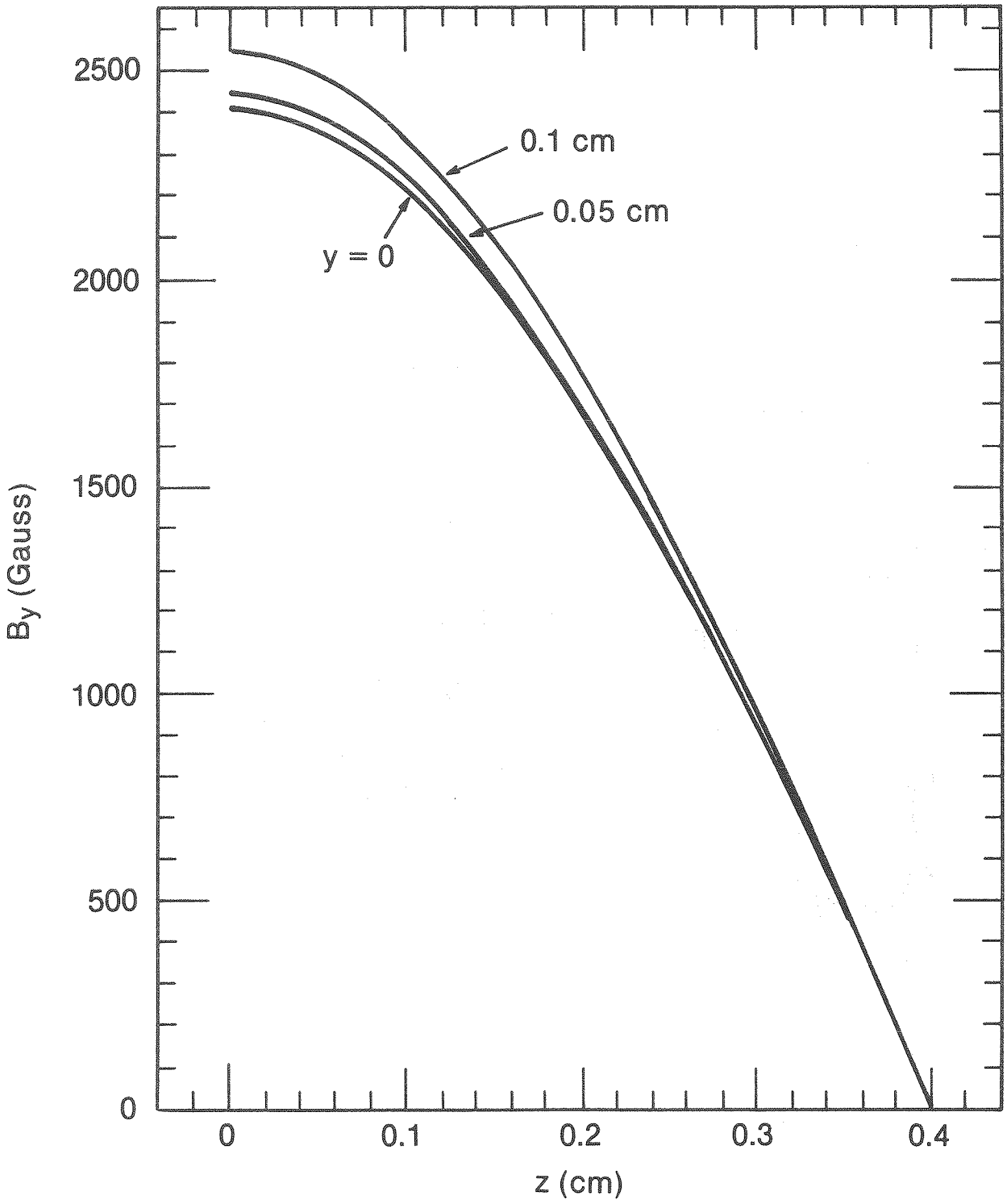

Fig. 23 Magnetic field variation along the z-axis over half-period of an undulator with λ_o=1.6 cm. The y values shown on the curves represent the position of the position trajectory above the undulator axis.

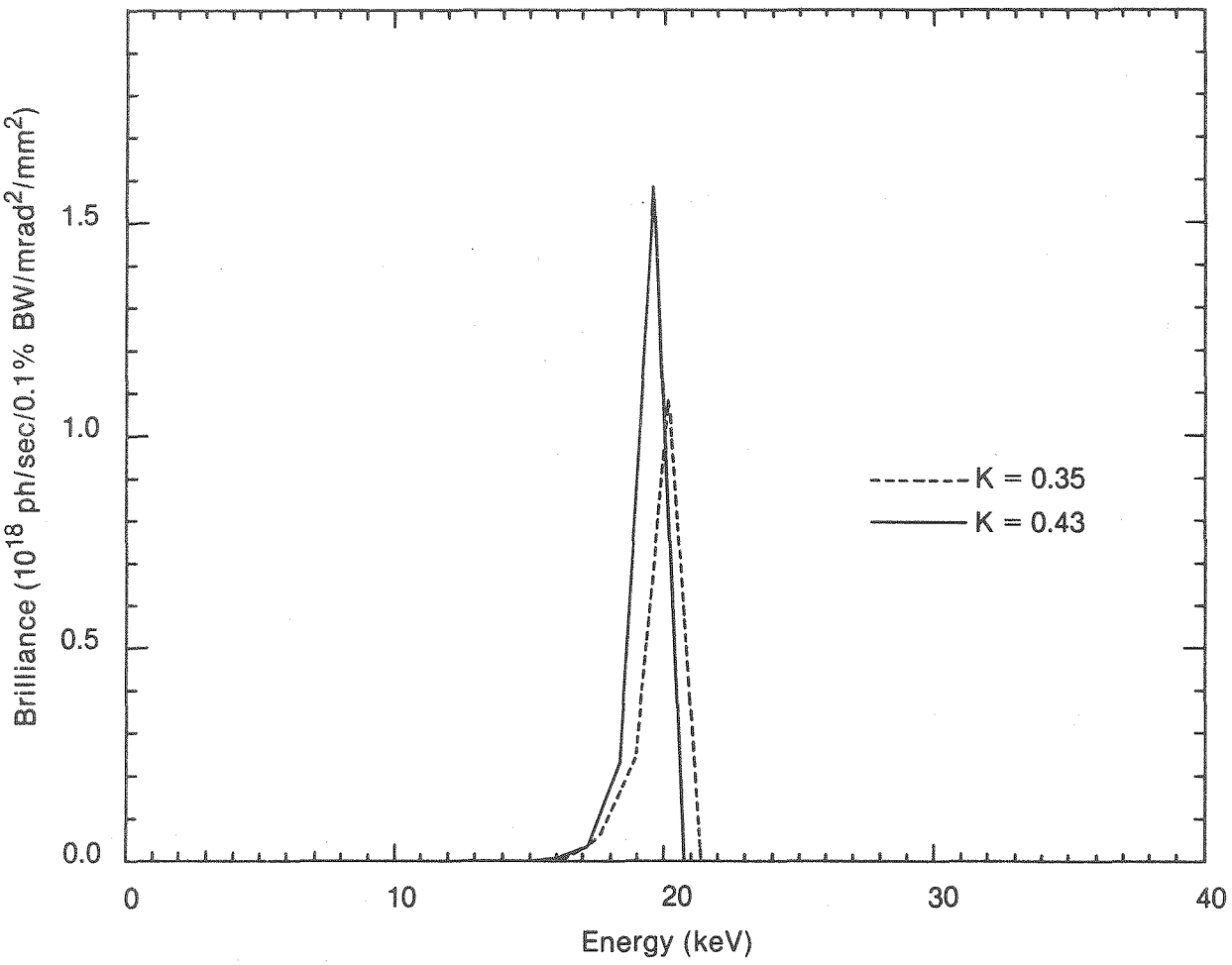

Fig. 24 Angle-integrated on-axis spectral brilliance of a 20 keV undulator with REC (K=0.35) and Nd-Fe-B (K=0.43) hybrid configurations

B chamber with an 8 mm aperture. The consequences of each choice were discussed in detail earlier. The following discussion is limited to the mechanical details of rigid undulator vacuum chambers and pumping chambers for this straight section. The halves of the rigid chamber will be machined to provide the needed geometry and welded together along the neutral axis to minimize warping.

The 5.2 m long undulator vacuum chamber will have pumping antechambers welded onto each side, as shown in Fig. 25. A Zr/Al getter pumping strip will be mounted inside each pumping chamber. Each slot will have a conductance of approximately 1.6 ℓ/sec (for nitrogen). Considering that only one side of the Zr/Al strip will be available for pumping, the initial effective pumping speed on each side of the undulator vacuum chamber at room temperature will be 50 and 150 ℓ/sec/meter of undulator length for CO and H_2, respectively.

13. A Wiggler-Undulator

13.1 Introduction

It would be very useful to have an ID which could provide a wide variability in K, and thus serve as both an undulator and a wiggler. Such a device would have many interesting applications, as it would permit different kinds of investigations to be carried out on a beamline without restructuring the ID. To demonstrate this capability in the case of the 6 GeV storage ring, a preliminary design is presented for a device with an 8 cm period. The variation in K for such a device as a function of G/λ_o is shown in Fig. 10.

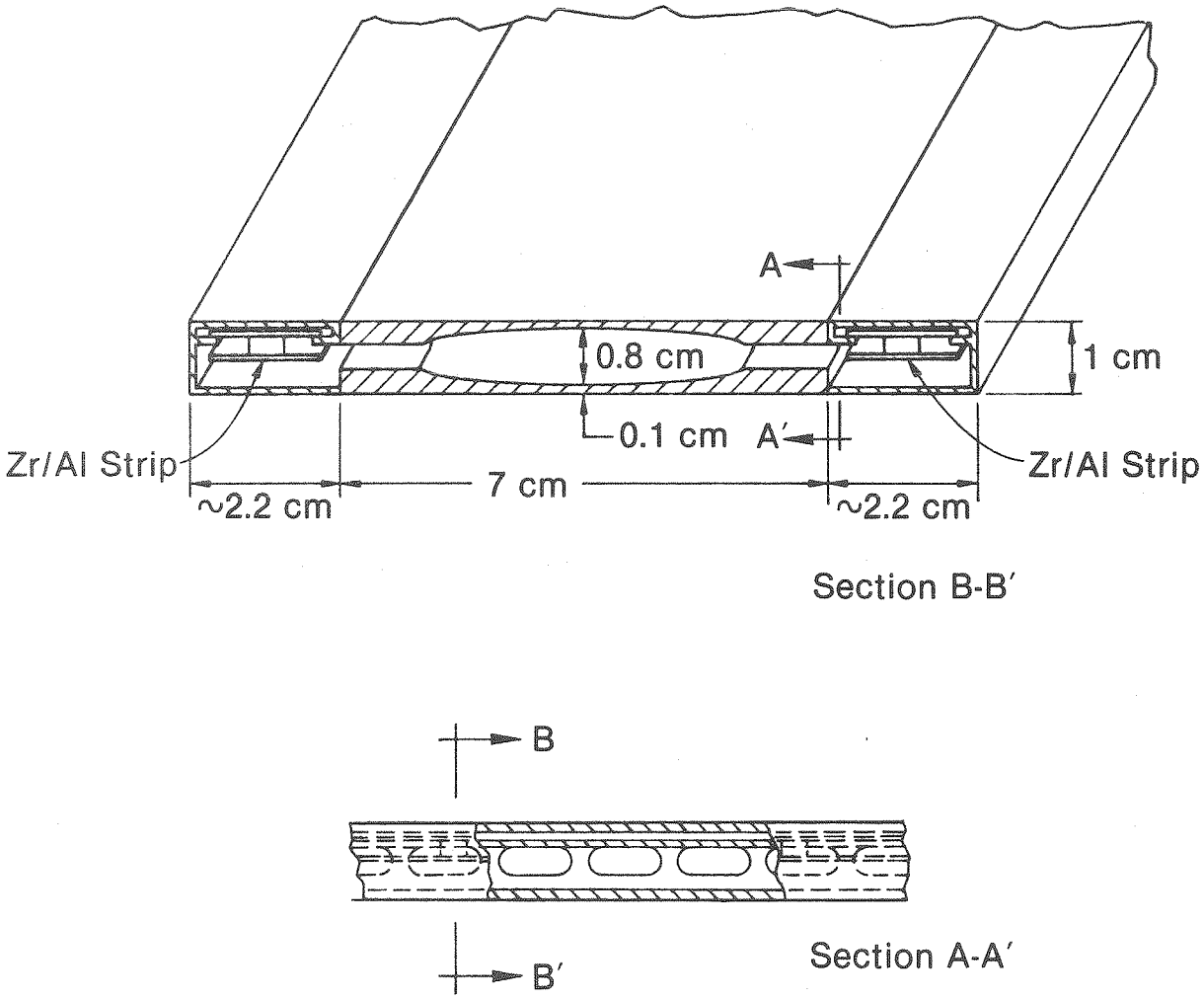

Fig. 25 Schematic of vacuum chamber, showing pumping chambers containing Zr/Al strips for the 20-keV undulator

13.2 Preliminary Design Parameters

The minimum gap needed for the device to be a wiggler is about 2.0 cm. With the hybrid REC configuration, we can achieve a K value of about 9. Under these conditions, design optimization need not be carried out to maximize the peak field at a gap of 2.0 cm. Instead, the aim of optimization is to achieve the desired field or deflection parameter K at a gap of 2.0 cm, and minimize the aspect ratio (height/thickness) of the magnetic material. Also, the magnetic-field quality with a cosine-functional variation is not important at smaller gaps at which the ID behaves as a wiggler.

On the other hand, at gaps larger than 4 cm, the device has undulator characteristics, with K varying between 1 and 2. Hence the two-dimensional field optimization discussed in Section 12.2 was carried out for gap values ranging from 4.0 to 5.6 cm. The results of this iterative optimization are presented in Table 9.

Figure 26 shows the optimized two-dimensional magnetic flux configuration of a quarter-period of the ID for a gap of 4 cm. The variation obtained in the y-component of the magnetic field from the optimization at G = 4 cm is shown in Fig. 27. In addition, the field profile for a trajectory located at y = 0.2 cm is shown. The deviation here is much smaller than that computed for the small-period undulator discussed in Section 12.2.

The angle-integrated on-axis brilliance for this device is shown in Fig. 28 for two different values of K as a function of photon energy. The first-harmonic energy peaks for the two cases are located at 1.5 and 2.5 keV, respectively.

A type A vacuum chamber (as discussed in Section 9.8) can be used for this device, and the pumping chambers can be incorporated as discussed in Section 12.3.

Table 9

Optimized Parameters of the Hybrid REC Wiggler-Undulator

Undulator Period, λ_o (cm)	8.0
Magnet Gap, G (cm)	2.0 to 5.6
Pole Width (cm) in x Direction	11.0
Pole Height (cm) in y Direction	4.25
Pole Thickness (cm) in z Direction	2.0
Magnet Width (cm) in x Direction	13.0
Magnet [Tnqvti ¶b"< in y Direction	4.5
Magnet Thickness (cm) in z Direction	6.0
Pole-Tip Overhang (cm) in y Direction	0.25
Peak Field On Axis, B_o (T)	1.2 to 0.15
Peak K On Axis	9 to 1
Peak Field Increase (%) at 0.2 cm Off Axis in y Direction at G = 4 cm	0.4
Length of Straight Section (m)	6.0
Minimum Length of Transition Section (m)	0.4
Maximum Length Available for Undulator (m)	5.2
Maximum Undulator Periods Used in Spectral Calculations, N	62

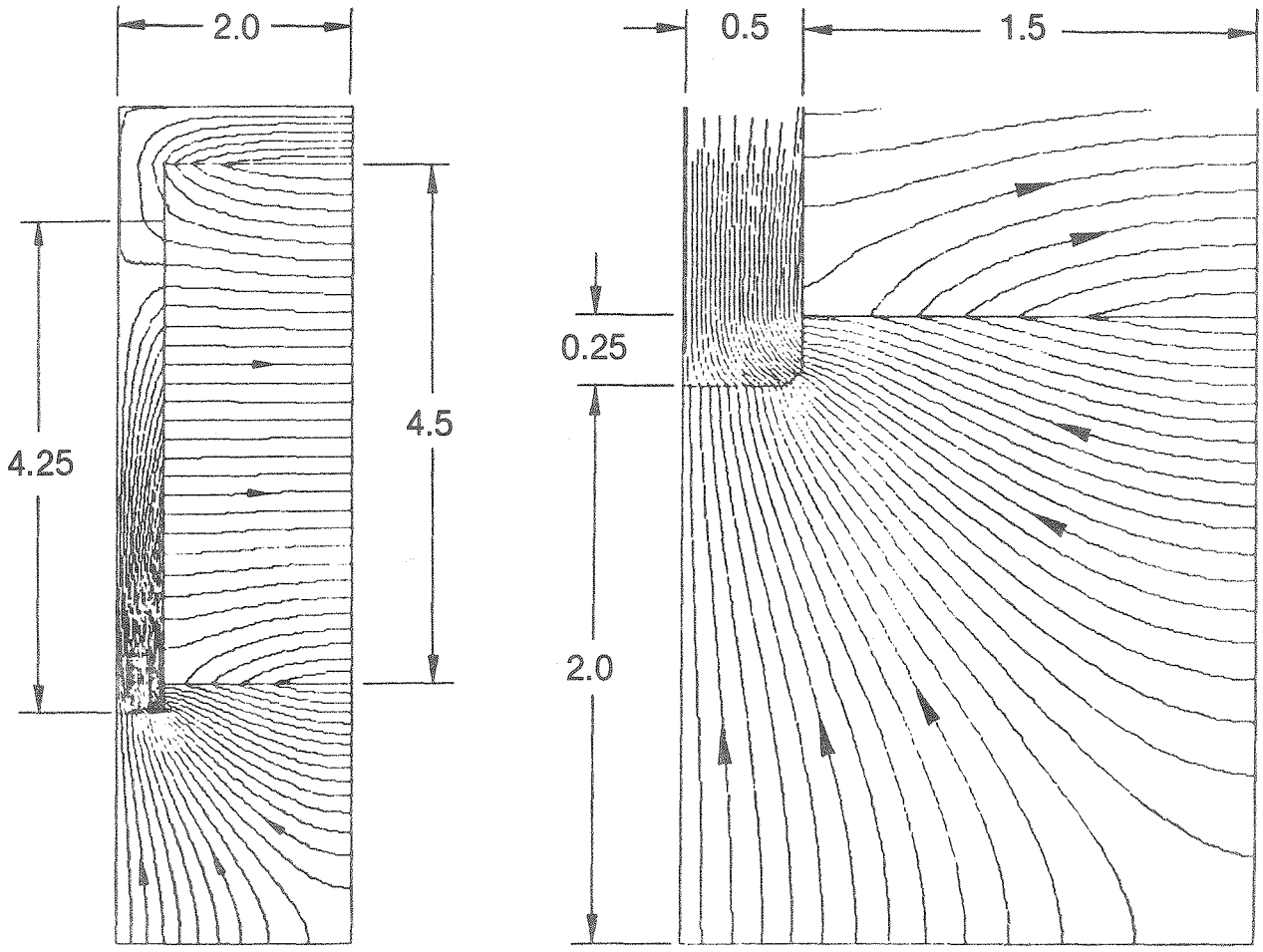

Fig. 26 Magnetic flux distribution in a quarter period of an optimized undulator used for soft x-ray radiation with a G=4 cm and λ_o=8 cm. Dimensions are in cm. The view on the right is an expanded portion of the pole overhang region discussed in the text.

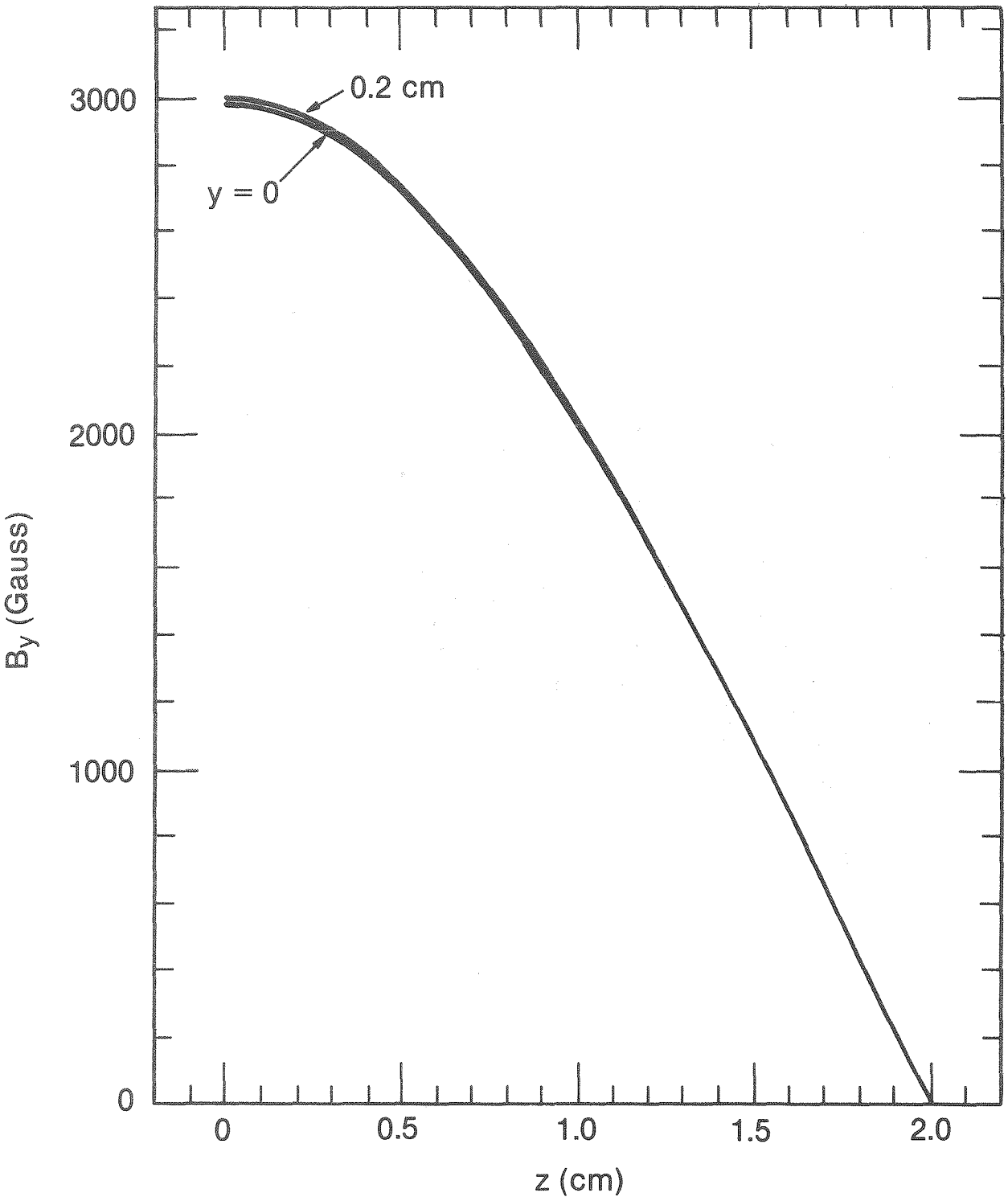

Fig. 27 Magnetic field variation for two values of y for an optimized undulator with G=4 cm and λ_o=8 cm

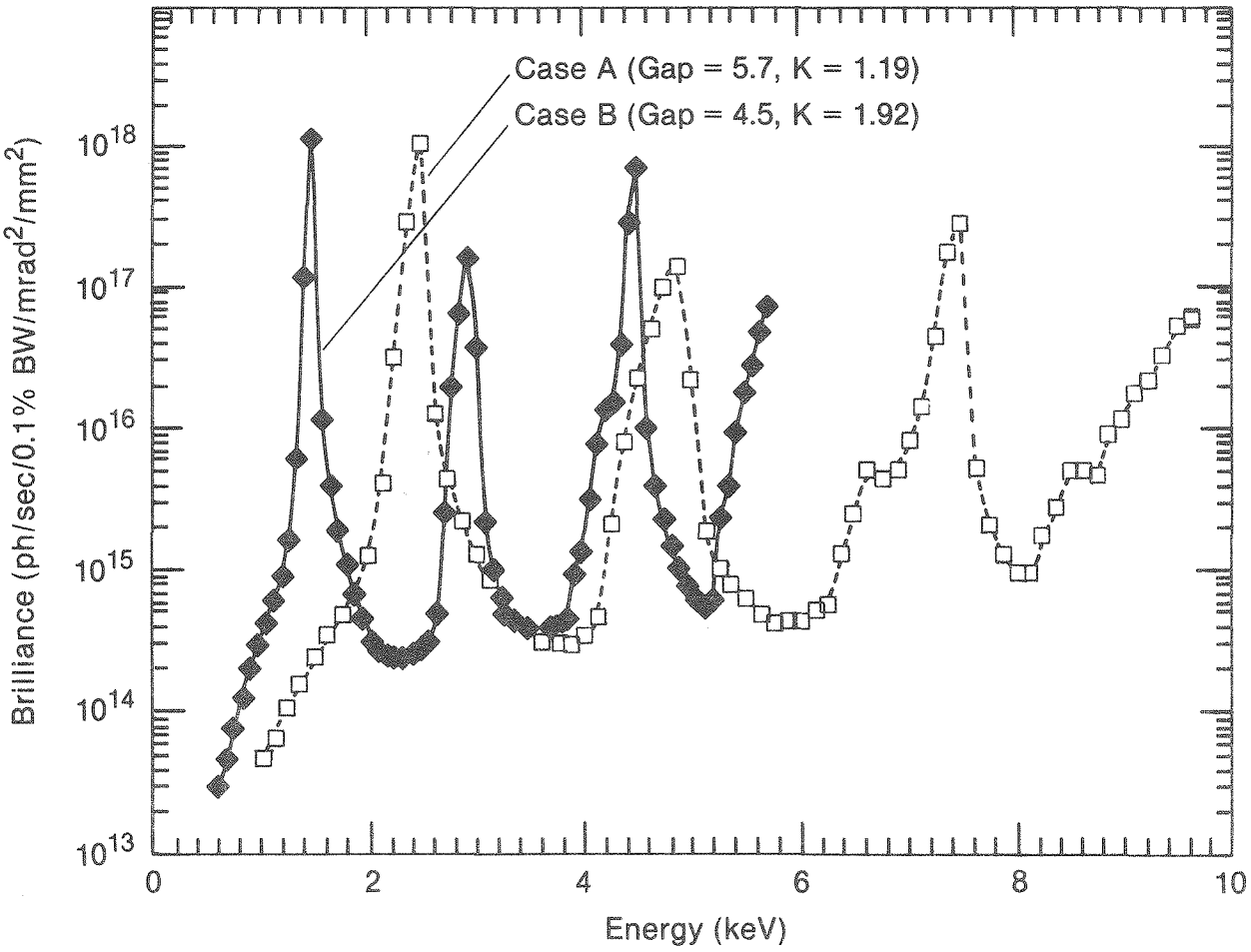

Fig. 28 Angle-integrated on-axis spectral brilliance vs. energy for an undulator with λ_o=8 cm and two different values of K. These calculations include the source size.

REFERENCES

1. G. K. Shenoy and P. J. Viccaro, "An Overview of the Characteristics of the 6 GeV Synchrotron Radiation: A Preliminary Guide for Users," ANL Report ANL-85-69 (October 1985).

2. "Conceptual Design of Sample Beamlines and Facilities for the 6 GeV Synchrotron Source," ANL Report, Light Source Note LS-51 (1986)